

Velocity Enhancement Models for Polymer Flooding in Reservoir Simulations

by

E. Guarnerio

Literature Study Report
at the Delft University of Technology

Student number: 4747259

Supervisor: Dr. ir. J.E. Romate, TU Delft and & Shell Global Solutions Internationals

Contents

1	Introduction	1
2	Hyperbolic Conservation Laws	3
2.1	Introduction to Conservation Laws	3
2.2	The Riemann Problem	6
2.3	Discontinuous Flux Function	8
2.3.1	The Riemann Problem for Discontinuous Flux Function	8
3	A Glossary of Petroleum Terms	11
3.1	Reservoir Rock Properties	11
3.2	Reservoir Fluid Properties	11
3.3	Reservoir Rock/Fluid Properties.	12
4	Multi-Phase Flow in Porous Media	17
4.1	Mass Conservation	17
4.2	Fractional Flow Formulation	19
4.3	Polymer Flood	20
4.3.1	Thick Water Model	22
4.3.2	Extended Fractional Flow Theory	23
5	Velocity Enhancement Models for Polymer Flooding	27
5.1	Inaccessible and Excluded Pore Volumes	27
5.2	Models for the Velocity Enhancement Factor	29
5.2.1	Constant Velocity Enhancement Factor	30
5.2.2	Percolation Model.	32
5.2.3	Hilden-Nilsen-Raynaud Model	36
5.2.4	Conclusions	43
6	Overview of Numerical Methods	45
6.1	Numerical Methods for Waterflooding	45
6.2	Numerical Methods for Inert Tracer	47
6.3	Numerical Methods for Polymer Flooding	52
6.4	Remarks on Velocity Enhancement Factor	53
	Bibliography	55

1

Introduction

It is needless to state the importance of oil in the world economy, as it is one of the primary source of energy worldwide. Many different techniques are applied to maximize the amount of oil that can be extracted from a reservoir. During the producing life of a reservoir, three phases are usually distinguished: primary, secondary and tertiary recovery. Primary recovery is driven by natural mechanisms, such as fluid expansion due to pressure decline, and no injection process is involved. The absence of water injection in the production makes this phase the most profitable one of the reservoir's life. Once the pressure drops below a certain limit, usually water or gas are injected to maintain a higher pressure and also to sweep out oil through a displacement process. This is known as the secondary recovery. However, oil is left behind in a waterflood either because it is trapped by capillary forces, or because it is bypassed by the water, which has a higher mobility and may find a path through the reservoir. At this point, at the production well, water is also produced and the method becomes inefficient and uneconomical. All the other techniques used after waterflooding are tertiary recovery. The nature of the recovery is now based on displacement of the oil. These techniques includes thermal, solvent and chemical methods. In general, Enhanced Oil Recovery (EOR) are all the techniques for oil recovery that involve the injection of materials not normally present in the reservoir. This definition does not restrict EOR to a particular phase of oil recovery. The purpose of EOR is thus to displace the amount of oil which is unrecoverable through conventional methods.

In this work, the focus will be on polymer flooding, that is, polymer is added to the injected water in order to increase its viscosity, resulting in a more favourable mobility ratio M , defined as

$$M = \frac{\lambda_w}{\lambda_o} = \frac{k_{r,w}\mu_o}{k_{r,o}\mu_w},$$

where λ, μ and k_r are the mobility, viscosity and relative permeability respectively, and the subscripts o and w refer to oil and water phase. A lower mobility ratio will improve the oil displacement performed by the solution water-polymer. In order to study polymer flooding from a theoretical point of view, a mathematical model for the flow of a fluid in a reservoir (a porous media) is needed. The complexity of these models raises rather quickly as more physical and chemical factors are considered, thus it is essential to state reasonable assumptions to simplify the models to allow for analytical study and numerical simulations of the flow.

The report will be structured as follows: in chapter 2, general theory for hyperbolic equations is discussed. The governing equations of the presented models are mainly

in hyperbolic form, so a good understanding of the main features of the solution of these equations, such as rarefaction and shock waves, is necessary. In Chapter 3, a glossary of petroleum terms is given, so that the reader will become familiar with the chemical and physical properties of a reservoir. In Chapter 4, the basic theory and equations of fluid's flow in porous media are discussed, including the fractional flow formulation derived by Buckley-Leverett, which is used in a wide range of models and simulators. Chapter 5 will focus on the discussion of more advanced models of specific use for polymer flooding. Here, the inaccessible pore volume (IPV) effect will be discussed: since the polymer molecules are larger, they will not enter all the pores available for water, so that the polymer may travel faster than an inert tracer. As a consequence, velocity enhancement models are considered. These models must be though treated with caution since, as it will be shown, they can lead to ill-posed problems, in particular a non physical pile-up of the polymer at the water front is observed in numerical simulations. Last, an overview of numerical methods will be carried out in Chapter 6, focusing on finite volume method with upwind schemes for fluxes.

2

Hyperbolic Conservation Laws

Hyperbolic laws arise in many different applications. They have a central importance also in EOR, especially in water and polymer flooding, where even basic models for fluid's flow present typical features related to its hyperbolic nature. Thus, a complete understanding of the peculiarities of the solutions that are generated, such as rarefaction waves and discontinuities (often referred to as shocks), is essential. For an introduction to conservation laws, the reader is referred to Salsa [12]. For sections 2.2 and 2.3, the approach of Holden-Risebro [4] will be followed; since a thorough discussion would take too much time, one should refer to this text for details.

2.1. Introduction to Conservation Laws

The general form of a scalar conservation law is

$$u_t + f(u)_x = 0, \quad x \in \mathbb{R}, t > 0, \quad (2.1)$$

where $f \in C^1$ is usually referred to as the flux function and u represents some physical property such as concentration. Equation (2.1) and the initial condition

$$u(x, 0) = u_0(x), \quad x \in \mathbb{R}. \quad (2.2)$$

together form an initial value (or Cauchy) problem.

The method of characteristic is used to build the solution of this kind of problems: it is possible to find curves on the (x, t) -plane for which u is constant. That is, curves of the form $x = \xi(t; x_0)$ where

$$\frac{d}{dt}u(\xi(t; x_0), t) = 0.$$

Let us consider the Cauchy problem in the case of linear equation

$$\begin{cases} u_t + au_x = 0 & x \in \mathbb{R}, t > 0 \\ u(x, 0) = u_0(x) \end{cases} \quad (2.3)$$

where $a > 0$ is a given constant. For this simple case, the characteristic are of the form $\xi(t; x_0) = at + x_0$. Indeed,

$$\frac{d}{dt}u(\xi(t; x_0), t) = \frac{d}{dt}u(x(t), t) = u_t + au_x = 0.$$

The initial data $u_0(x)$ is then transported along the characteristics, where $u(x, t)$ is constant. Formally,

$$u(\xi(t; x_0), t) = u(\xi(0; x_0), 0) = u(x_0, 0) = u_0(x_0),$$

meaning, more explicitly,

$$u(at + x_0, t) = u_0(x_0).$$

Rewriting $x = at + x_0$ and $x_0 = x - at$ gives the solution to problem (2.3):

$$u(x, t) = u_0(x - at).$$

In the linear case studied above, the characteristics do not intersect and the solution is well defined in every point (x, t) . In the more general case (2.1), the method of characteristic is still applied, but a more precise analysis would show that, even with regular initial data, singularities may arise within the solution.

The equation for the characteristics reads

$$x(t) = f'(u_0(x_0))t + x_0, \quad f' = \frac{df}{du}.$$

To compute $u(x, t)$, consider the characteristic through (x, t) and follow it backward in time to determine the point $(x_0, 0)$. One then has $u(x, t) = u_0(x_0)$. Substituting the equation for the characteristic in the latter gives

$$u(x, t) = u_0(x - f'(u_0(x_0))t),$$

which can be rewritten as

$$u = u_0(x - f'(u)t).$$

Note that the last expression determines u implicitly.

The slope of the characteristics depend on the initial data u_0 and on $f'(u)$. It is clear then that existence and uniqueness of the solution in every point is not ensured, since the characteristics may intersect or be absent from a part of the (x, t) -plane. To deal with these situations, it is necessary to introduce a more flexible definition of solution which allows for discontinuities along the characteristics.

Definition 2.1. A function u , bounded in $\mathbb{R} \times [0, \infty)$, is called a weak solution to problem (2.1)-(2.2) if, for every test function $\varphi \in C_0^\infty(\mathbb{R} \times [0, \infty))$ it holds

$$\int_0^\infty \int_{\mathbb{R}} (u\varphi_t + f(u)\varphi_x) dx dt + \int_{\mathbb{R}} u_0\varphi(x, 0) dx = 0.$$

The subscript in C_0^∞ stands for compact support of the test function $\varphi(x, t)$. A classical solution is also a weak solution. Definition (2.1) seems quite flexible, since it allows for discontinuous solutions. It is though necessary to understand the behaviour of a weak solution through such discontinuity. A discontinuity, referred to as shock, arises when the characteristic through a point is not unique, as depicted in Figure 2.1

To determine the shock wave $s(t)$, a condition (Rankine-Hugoniot condition) is used:

$$\frac{ds}{dt} = \frac{f(u_r(s, t)) - f(u_l(s, t))}{u_r(s, t) - u_l(s, t)}. \quad (2.4)$$

Here, u_r and u_l stand for the solution u immediately right and immediately left of the shock, respectively. Along with an appropriate initial condition (in the case depicted

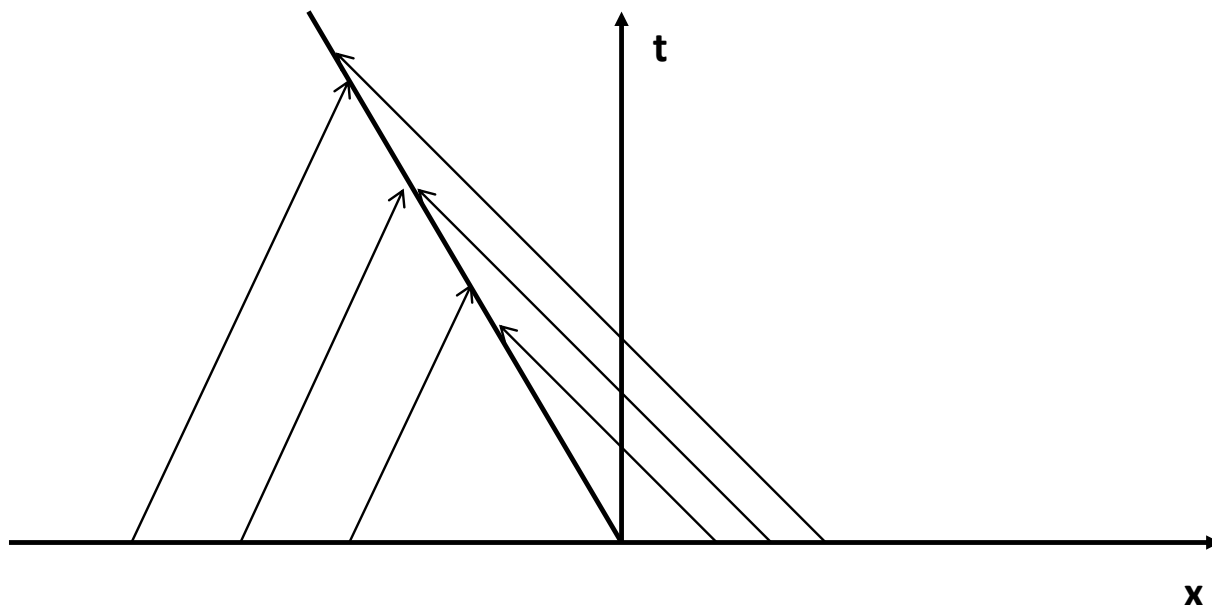


Figure 2.1: Characteristics collide: generation of a shock wave.

in Figure 2.1 it would be $s(0) = 0$), (2.4) determines the equation for the shock wave $s(t)$. The solution u along the shock jumps from u_l to u_r .

To illustrate a case when rarefaction waves occur, consider Figure 2.2.

No characteristics enter the central region: an alternative way must be found to define a solution in such region. One can show that the following formula gives the solution in a region where rarefaction waves (centered at $x = 0$) occur:

$$u(x, t) = r\left(\frac{x}{t}\right), \quad r = (f')^{-1}. \tag{2.5}$$

The fan of characteristics is depicted in Figure 2.3.

Rarefaction and shock waves seem to ensure existence of a solution in the different configurations that may occur. What about uniqueness?

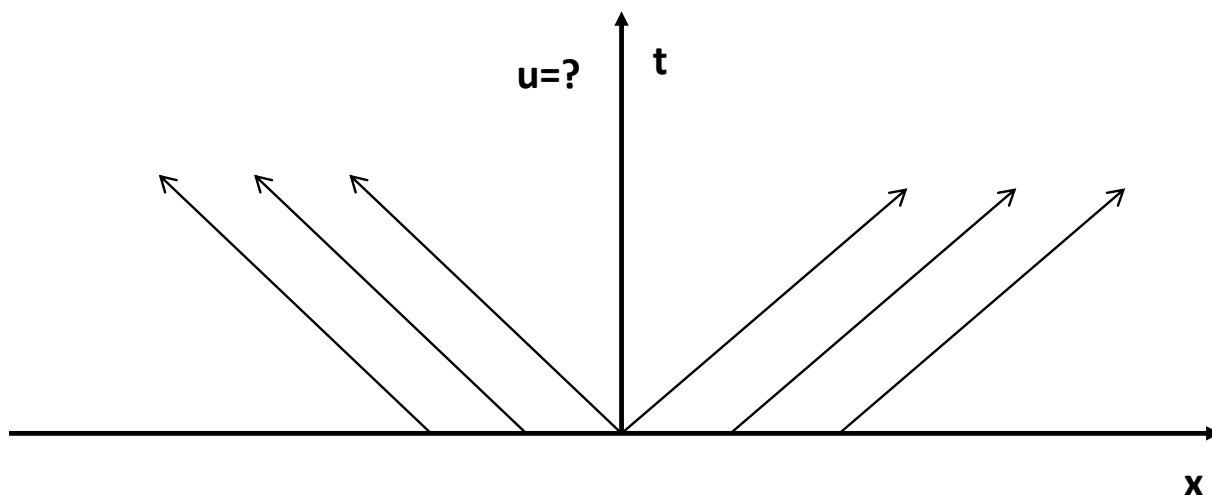


Figure 2.2: No information in the central region: generation of a rarefaction wave.

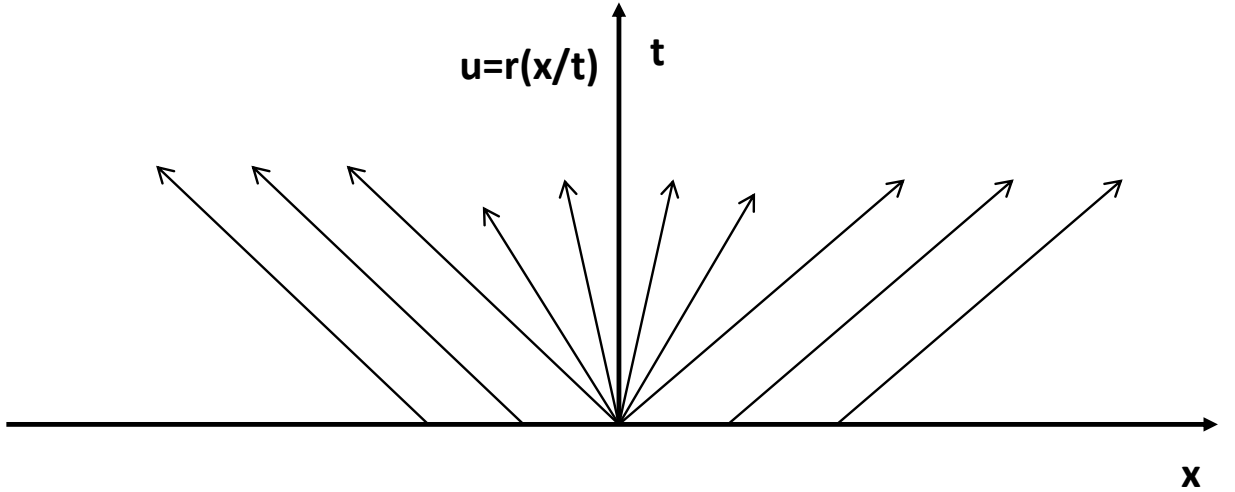


Figure 2.3: Rarefaction wave centered in the origin.

There are cases where both rarefaction and shock waves can be built to define a (weak) solution, so one may wonder if further conditions can be derived to ensure uniqueness. To this purpose, it is convenient to think of a physical interpretation of the solution. These solutions are referred to as entropy solutions, related to the study of gas dynamic. There are various ways to formulate an entropy condition. One of the most common is the viscous regularization: equation 2.1 is replaced by

$$u_t + f(u)_x = \epsilon u_{xx}. \quad (2.6)$$

Note that (2.6) is a parabolic equation, thus, even if ϵ is small, the equation has a much more regular behaviour. The idea is that, physically, a model is more realistic if some diffusion is taken into account, and a conservation law represents a limit model when diffusion goes to zero. A unique solution for (2.1) is selected such that it satisfies equation (2.6) for the limit $\epsilon \rightarrow 0$.

One can show that, for sufficiently regular solutions, this entropy condition is equivalent to the *Kružkov* entropy condition. A solution satisfies a *Kružkov* entropy condition if

$$\iint (\eta(u)\phi_t + q(u)\phi_x) dx dt \geq 0 \quad (2.7)$$

holds for all convex functions η and all nonnegative test functions $\phi \in C_0^\infty(\mathbb{R} \times (0, \infty))$. It is often more convenient to work with this condition to show that solutions satisfy entropy conditions.

2.2. The Riemann Problem

Studying a particular initial value problem, the Riemann problem, gives useful insights on the behaviour of problems with more complicated initial value. The information contained in this section are based on the work of Holden-Risebro [4].

The Riemann problem is the initial value problem

$$u_t + f(u)_x = 0, \quad u(x, 0) = \begin{cases} u_l & \text{for } x < 0 \\ u_r & \text{for } x \geq 0. \end{cases} \quad (2.8)$$

Since both the equation and initial data are invariant under the transformation $x \mapsto kx$ and $t \mapsto kt$, it makes sense to look for solution of the form $u(x, t) = w(x/t)$.

Assuming for a moment that $f \in C^2$ and substituting into the equation yields

$$-\frac{x}{t^2}w' + \frac{1}{t}f'(w)w' = 0. \quad (2.9)$$

Setting $z = x/t$, equation (2.9) can be rewritten as

$$z = f'(w), \quad (2.10)$$

which has the simple solution $w = (f')^{-1}(z)$ if f' is strictly monotone. Of course, in general the monotonicity of f' cannot be guaranteed, thus f' must be replaced by a monotone function on the interval between u_l and u_r . Assume now that $u_l < u_r$. On the interval $[u_l, u_r]$, f is replaced by its lower convex envelope f_- , defined by

$$f_-(u) = \sup\{g(u) \mid g \leq f \text{ and } g \text{ convex on } [u_l, u_r]\}. \quad (2.11)$$

An example of a convex envelope is shown in Figure 2.4.

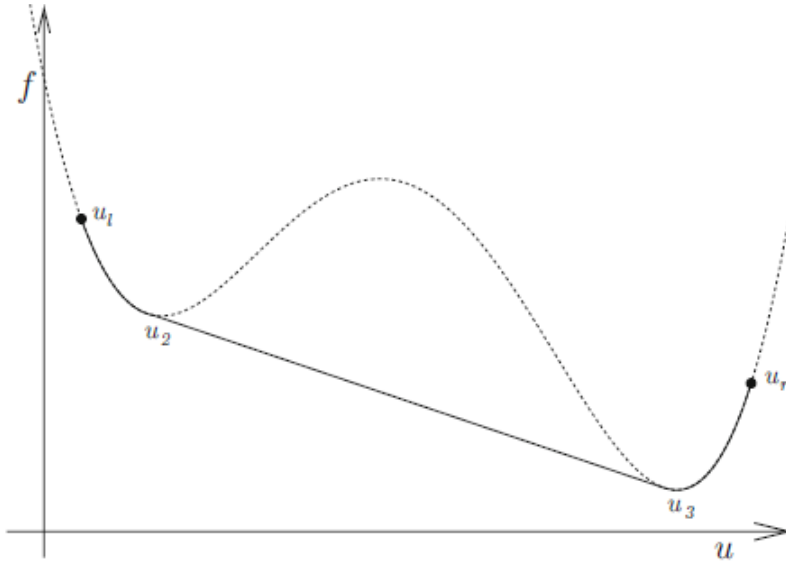


Figure 2.4: Convex envelope of f in the interval $[u_l, u_r]$. From [4].

One can show that a solution to (2.8) satisfying a Kružkov entropy condition is given by

$$u(x, t) = w(z) = \begin{cases} u_l & \text{for } x \leq f'_-(u_l)t, \\ (f'_-)^{-1}(x/t) & \text{for } f'_-(u_l)t \leq x \leq f'_-(u_r)t, \\ u_r & \text{for } x \geq f'_-(u_r)t, \end{cases} \quad (2.12)$$

for $u_l < u_r$ and denoting $(f'_-)^{-1} = ((f_-)')^{-1}$. Note that $f'' \geq 0$, thus f' is nondecreasing. Permitting jump discontinuities where f' is constant, its inverse can be defined, so (2.12) makes sense. If $f \in C^2$ has finitely many inflection points, there will be finitely many intervals where, alternately, $f_- = f$ or $f_- < f$. In this case, $u(x, t)$ will have the form $u(x, t) = (f')^{-1}(x/t)$, with a finite number of discontinuities corresponding to the intervals where $f_- < f$. At such discontinuity points, it holds

$$x = f'(u_j)t = \frac{f(u_{j+1}) - f(u_j)}{u_{j+1} - u_j}t = f'(u_{j+1})t, \quad (2.13)$$

where on the interval $[u_j, u_{j+1}]$ it holds $f_- < f$. Expression (2.13) satisfies the Rankine-Hugoniot condition. Hence, the solution given by (2.12) is a sequence of rarefaction waves alternating with shock waves. In Figure 2.4, there are three intervals, where $f_- < f$ on the middle one $[u_2, u_3]$. Thus, there will be a rarefaction wave for $f'_-(u_l)t \leq x \leq f'_-(u_2)t$, followed by a shock wave satisfying (2.13) with $j = 2$, and again rarefaction wave for $f'_-(u_3)t \leq x \leq f'_-(u_r)t$ (in this case, $f'_-(u_2) = f'_-(u_3)$).

If instead $u_l > u_r$, one can consider the transformation $x \mapsto -x$ and the alternative Riemann problem

$$u_t - f(u)_x = 0, \quad u(x, 0) = \begin{cases} u_r & \text{for } x < 0 \\ u_l & \text{for } x \geq 0. \end{cases} \quad (2.14)$$

Following the same procedure, it is necessary to build the convex envelope of $-f$ from u_r to u_l . This is exactly the negative of the upper concave envelope from u_r to u_l . The concave envelope of f is defined by

$$f_-(u) = \inf\{g(u) \mid g \geq f \text{ and } g \text{ concave on } [u_r, u_l]\}. \quad (2.15)$$

Analogously to (2.12), the solution is now

$$u(x, t) = w(z) = \begin{cases} u_l & \text{for } x \leq f'_-(u_l)t, \\ (f'_-)^{-1}(x/t) & \text{for } f'_-(u_l)t \leq x \leq f'_-(u_r)t, \\ u_r & \text{for } x \geq f'_-(u_r)t. \end{cases} \quad (2.16)$$

This construction of the solution is valid as long as $f_{-, \sim} \neq f$ on finitely many intervals, alternating with intervals where $f_{-, \sim} = f$. The solution can be extended to the case in which f is a piecewise twice differentiable function. Furthermore, next section will extend the analysis to the case of a discontinuous flux function. The results of this section can be summarized in the following theorem (Holden-Risebro [4]).

Theorem 2.2. *The initial value problem (2.8) with a flux function $f(u)$ such that $f_{-, \sim} \neq f$ on finitely many intervals, alternating with intervals where they coincide, has a weak solution given by (2.12) if $u_l < u_r$, or by (2.16) if $u_r < u_l$. This solution satisfies the Kruřkov entropy condition.*

2.3. Discontinuous Flux Function

In water and polymer flooding, physical phenomena and processes may be modeled by conservation laws. In such equations, it will be shown that cases with a discontinuous flux function $f(u)$ will arise. It is thus convenient to study the Riemann problem for such functions, in order to understand the behaviour of the solution and derive conditions to have a well-posed problem. Holden and Risebro [4] studied this kind of problems, proposing a way to build an entropic solution. They investigated further existence and uniqueness of entropy solutions for more general Cauchy problems, but such discussion is not needed for the models presented later and it will be omitted.

2.3.1. The Riemann Problem for Discontinuous Flux Function

The Riemann problem studied in this section is

$$\begin{cases} u_t + f(\gamma_l, u)_x = 0, & u(x, 0) = u_l, & \text{for } x < 0, \\ u_t + f(\gamma_r, u)_x = 0, & u(x, 0) = u_r, & \text{for } x > 0, \end{cases} \quad (2.17)$$

where γ_l, γ_r, u_l and u_r are constants. The first thing to show is that, under some regularity assumptions on f , weak solutions exist, and the fulfillment of an additional entropy condition yields uniqueness.

To find a solution to (2.17), the starting point is to observe that $u(x, t)$ must be the solution to two problems, one on the positive x -plane and one on the negative x -plane, namely

$$v_t + f(\gamma_l, v)_x = 0, \quad v(x, 0) = \begin{cases} u_l & \text{for } x < 0, \\ u'_l & \text{for } x = 0, \end{cases} \quad (2.18)$$

and

$$w_t + f(\gamma_r, w)_x = 0, \quad w(x, 0) = \begin{cases} u'_r & \text{for } x = 0, \\ u_r & \text{for } x > 0. \end{cases} \quad (2.19)$$

The values u'_l, u'_r are yet to be determined. The solution to (2.17) is then built by gluing together solutions to (2.18) and (2.19):

$$u(x, t) = \begin{cases} v(x, t), & \text{for } x < 0, \\ w(x, t), & \text{for } x > 0. \end{cases} \quad (2.20)$$

To make sure that this construct is possible, $v(0-, t)$ and $w(0+, t)$ have to satisfy some extra conditions.

In the previous section, it was shown that the solution to the Riemann problem

$$v_t + g(v)_x = 0, \quad v(x, 0) = \begin{cases} v_l & \text{for } x < 0, \\ v_r & \text{for } x \geq 0, \end{cases}$$

is found constructing the lower convex or upper concave envelope, depending whether $v_l < v_r$ or $v_l > v_r$. Introducing the notation

$$\bar{g}(v; v_l, v_r) = \begin{cases} g_-(v; v_l, v_r) & \text{if } v_l < v_r, \\ g_+(v; v_l, v_r) & \text{if } v_l > v_r, \end{cases} \quad (2.21)$$

the solution for $\bar{g}'(v_l; v_l, v_r)t \leq x \leq \bar{g}'(v_r; v_l, v_r)t$, satisfying the entropy condition, is

$$v(x, t) = \bar{g}'^{-1}\left(\frac{x}{t}; v_l, v_r\right).$$

Since the solution to (2.17) is formed by gluing together v and w , then v must be equal to u'_l for $x > 0$ (thus allowing only waves with nonpositive speed), while w must be equal to u'_r for $x < 0$ (thus allowing only waves with nonnegative speed). These observations follow by the fact that Riemann problems have similarity solutions, i.e. solutions of the form $u(x, t) = s(x/t)$, as discussed in the previous section. The solution will then be constant along any ray x/t through the origin, so at $x = 0$ the solution keeps the same value. Furthermore, since v contains only waves propagating to the left (nonpositive) and w contains only waves propagating to the right (nonnegative), the jump at $x = 0$ has zero speed. The Rankine-Hugoniot condition yields

$$\frac{f(\gamma_l, u'_l) - f(\gamma_r, u'_r)}{u'_l - u'_r} = 0,$$

so that

$$f(\gamma_l, u_l') = f(\gamma_r, u_r'). \quad (2.22)$$

These considerations are used to determine a set of values from which u_r' and u_l' must be chosen. The characterization of these sets is rather technical and it will not be presented here, the interested reader should refer to [4]. We only mention that uniqueness for u_l' and u_r' is ensured by an entropy-like condition motivated by the viscous regularization, as discussed in the previous section. The following theorem states that, under reasonable assumptions on $f(\gamma, u)$, the existence of a unique entropy solution is ensured.

Theorem 2.3. *Consider the Riemann problem*

$$\begin{aligned} u_t + f(\gamma, u)_x &= 0, \quad t > 0, \\ u(x, 0) &= \begin{cases} u_l & \text{for } x < 0, \\ u_r & \text{for } x > 0, \end{cases} \quad \gamma(x) = \begin{cases} \gamma_l & \text{for } x < 0, \\ \gamma_r & \text{for } x > 0. \end{cases} \end{aligned} \quad (2.23)$$

(i) *Let $f = f(\gamma, u)$ be a continuously differentiable function on the set*

$$(\gamma, u) \in [\gamma_1, \gamma_2] \times [u_1, u_2] = \Omega.$$

Assume that

$$\frac{\delta f}{\delta \gamma}(\gamma, u_1) = \frac{\delta f}{\delta \gamma}(\gamma, u_2) = 0,$$

so that $f(\gamma, u_1) = C_1$ and $f(\gamma, u_2) = C_2$ for some constants C_1 and C_2 . Then the Riemann problem (2.23) has a unique entropy solution for all (γ_l, u_l) and (γ_r, u_r) in Ω . Furthermore, $u(x, t) \in \Omega$ for all x and t .

(ii) *Let $f = f(\gamma, u)$ be a locally Lipschitz continuous function for $\gamma \in [\gamma_1, \gamma_2]$ and $u \in \mathbb{R}$. Assume that*

$$\lim_{u \rightarrow \pm\infty} f(\gamma, u) = \infty \quad \text{or} \quad \lim_{u \rightarrow \pm\infty} f(\gamma, u) = -\infty,$$

for all $\gamma \in [\gamma_1, \gamma_2]$. Then the Riemann problem (2.23) has a unique entropy solution for all (γ_l, u_l) and (γ_r, u_r) in $[\gamma_1, \gamma_2] \times \mathbb{R}$.

3

A Glossary of Petroleum Terms

Before starting to develop mathematical models for fluid flow in porous media, it is essential to be familiar with the physical and chemical properties that characterize both the rock and the fluid. These properties will influence the flow of the fluid through the rock. The main rock properties of interest are porosity and permeability, while for the fluid density, compressibility and viscosity will have relevant importance. In addition, the rock-fluid interaction properties will play an important role in the modeling. Material is taken from Chen [15].

3.1. Reservoir Rock Properties

The tiny empty passages in a rock are called *pores*. Typically, their size varies between 1 and $200\mu\text{m}$, depending on the rock layer. The *porosity*, usually indicated by ϕ , is the fraction of volume of rock which is pore space. One may further distinguish between total porosity and effective porosity: the latter includes only the pores which are interconnected, hence the ones responsible for fluid flow, while the total porosity includes also isolated pores. We shall consider effective porosity in the rest of the discussion. Porosity often varies in space, since in a reservoir different layers of rock may be present, but in many models will be considered constant for simplicity.

Permeability, denoted by k , measures the capacity of the rock to conduct fluids through its interconnected pores. This quantity is also known as *absolute permeability*, to distinguish it from the *relative permeability* that will be introduced later. A common unit for permeability is the *millidarcy* (md) ($1 \text{ darcy} \simeq 10^{-12}m^2$). Permeability usually varies on location and flow direction, but, in 3 dimensions, it is possible to assume it is a diagonal tensor. However, most of the models considered later are one-dimensional, so that the permeability k will be a scalar.

Often, porosity and permeability are positively correlated (figure 3.1): this result should not be surprising, since larger pores are most likely going to allow for more fluid to flow through the porous media.

3.2. Reservoir Fluid Properties

The main properties of fluids in a reservoir are now introduced.

A fundamental notion to be familiar with is the compressibility of a fluid: a fluid is classified as incompressible if its density is independent of pressure, otherwise it is said to be compressible. At reservoir condition the fluids may have a slightly

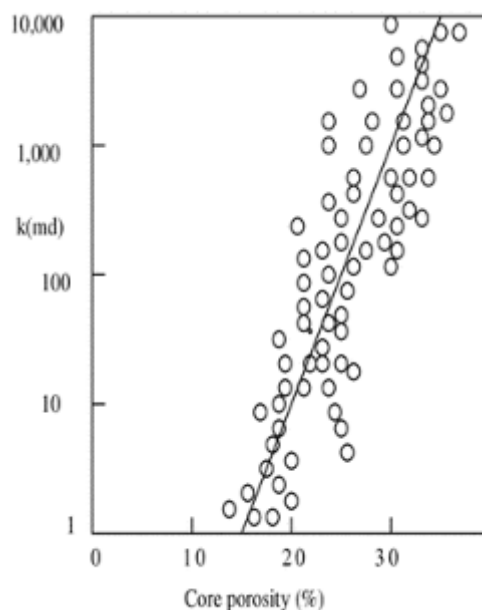


Figure 3.1: Permeability/porosity crossplot. From [15].

compressible behaviour, but often the assumption of incompressibility is used to derive mathematical models.

The *viscosity* of a fluid, denoted by μ , is a measure of the energy dissipated when it is in motion resisting an applied shearing force. It has the dimension of force/area and the most commonly used unit in field is *centipoise (cp)*. Viscosity is basically a consequence of the friction between the molecules of the fluid. In a gas, for example, where molecules are very far apart, viscosity will be low and the fluid will have a low resistance to flow. Most commonly, fluids called newtonian have constant viscosity.

3.3. Reservoir Rock/Fluid Properties

The interaction between the rock and the fluid is fundamental to derive realistic and appropriate models.

The first definition to be considered is *wettability*: the wettability of the rock measures the preference of the rock surface to be wetted by a particular phase. A formation which has a preference to be wetted by water is called *water wet*; an *oil wet* formation has a preference to be wetted by oil. The wettability influences other physical quantities, such as relative permeability and capillary pressure. This definition leads to the following characterization of a fluid displacement process:

- *Imbibition*: a displacement process where the wetting phase increases. In a water wet system, water flood will be an imbibition process: water will imbibe into a core containing mobile oil and occupy the smaller pores, thus displacing the oil.
- *Drainage*: a displacement process where the nonwetting phase increases.

Other properties, like capillary pressure and relative permeability, depend on the nature of the fluid displacement process.

A quantity widely used in the governing equations for fluid flow in porous media is the fluid phase *saturation*. The saturation, denoted by S , is the fraction of the pore space that a fluid phase occupies. For a two phase flow with oil and water, it holds

$$S_o + S_w = 1.$$

The *residual saturation* of a phase is the amount of that phase which is trapped and cannot be displaced, i.e. the fluid is immobile. For oil, this saturation is usually indicated as S_{or} (residual oil saturation), while for water the threshold value is called irreducible water saturation, S_{wir} . In the literature sometimes this saturation value is also referred to as connate water saturation S_{wc} , but there is a subtle yet important difference between the two terms: connate water saturation is more precisely defined as the fraction of water that remains trapped within sedimentary rocks during the process of sedimentation. This definition does not imply that connate water is immobile, although this will be the case in most of the reservoirs and many authors consider the connate water immobile.

Capillary pressure refers to the discontinuity between the pressure of the non-wetting phase, say oil, and the wetting phase, say water, thus taking the form

$$p_c = p_o - p_w. \quad (3.1)$$

Capillary pressure appears in a two-phase flow as a consequence of interfacial tension at the interface between the two immiscible fluids, such as oil and water. It depends on the saturation of the wetting phase and on its history (drainage or imbibition process), see figure 3.2. More accurate curves of the capillary pressure are obtained considering the dependence also surface tension σ , porosity ϕ , permeability k and the contact angle θ with the rock surface of the wetting phase. Using then the *J-function*

$$J(S_w) = \frac{p_c}{\sigma \cos \theta} \sqrt{\frac{k}{\phi}} \quad (3.2)$$

and performing experiments, typical curves are obtained.

In the case of three phase flow (say gas, oil, water), the capillary pressures are:

$$p_{cow} = p_o - p_w, \quad p_{cgo} = p_g - p_o, \quad p_{cgw} = p_g - p_w.$$

The capillary pressure p_{cgw} can be obtained from the previous ones as

$$p_{cgw} = p_g - p_w = p_{cow} + p_{cgo},$$

so that only two capillary pressures are needed.

Relative permeability is a dimensionless quantity (a fraction) that measures the effective permeability of a phase in the case of multiphase flow. In a two phase flow, one would expect the permeability to either fluid to be lower than that for the single fluid since it occupies only part of the pore space. Relative permeabilities depend on saturation and on the history of saturation change. In figure 3.3 typical relative permeabilities curves are depicted.

A number of models have been developed to relate relative permeability to other reservoir properties. A popular model for an analytic expression of relative permeabilities was proposed by Corey [8]:

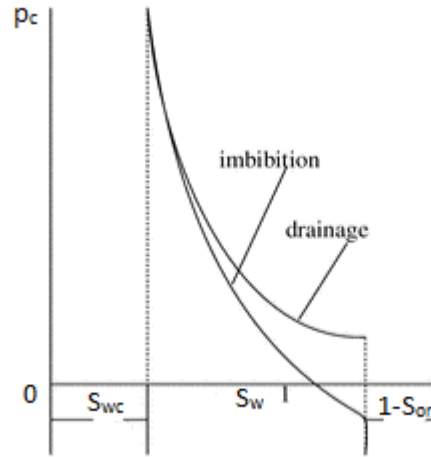


Figure 3.2: Typical capillary pressure curve. From [15].

$$k_{r,w} = \begin{cases} 0 & S_w \leq S_{wc}, \\ \left(\frac{S_w - S_{wc}}{1 - S_{wc} - S_{or}} \right)^{n_w} & S_{wc} < S_w < 1 - S_{or}, \\ 1 & S_w \geq 1 - S_{or}, \end{cases} \quad (3.3)$$

$$k_{r,o} = \begin{cases} 0 & S_w \leq S_{wc}, \\ \left(\frac{1 - S_w - S_{or}}{1 - S_{wc} - S_{or}} \right)^{n_o} & S_{wc} < S_w < 1 - S_{or}, \\ 1 & S_w \geq 1 - S_{or}, \end{cases} \quad (3.4)$$

where n_w , n_o are the Corey coefficients. The values of these coefficients can be chosen to capture the physical properties of the reservoir.

Relative permeability models for three phase flows are rather complicated and will not be discussed here, as the focus throughout the report will be on two phase systems.

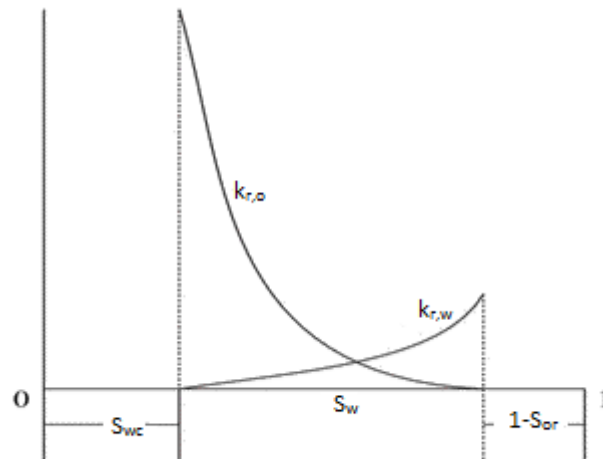


Figure 3.3: Typical relative permeabilities curves. From [15].

Next, it is useful to define the *mobility* λ_α and the fractional flow f_α of a phase α . The mobility is the ratio between relative permeability and viscosity of a certain

phase:

$$\lambda_w = \frac{k_{r,w}}{\mu_w}, \quad \lambda_o = \frac{k_{r,o}}{\mu_o}.$$

The mobility ratio M is the ratio between mobility of the displacing fluid and the mobility of the displaced fluid. For waterflooding:

$$M = \frac{\lambda_w}{\lambda_o}. \quad (3.5)$$

This is the quantity that polymer flood targets: polymer will increase water viscosity μ_w , resulting in a smaller (and more favourable) mobility ratio.

The interstitial velocity of the flowing phase is denoted by v_α . In the derivation of the model for the flow through the porous medium, it is common to work with the superficial (or Darcy) velocities $u_\alpha = \phi v_\alpha$. The reason is that an empirical law for u_α has been discovered by the French engineer Henry Darcy in 1856. Such law will be illustrated in the next chapter. Note that it holds $u_\alpha \leq v_\alpha$.

The fractional flow is a quantity that determines the (fractional) volumetric flow rate of a phase in the presence of another phase. The fractional flow of a phase is expressed as the ratio between the Darcy velocity of that phase and the total Darcy velocity $u = u_o + u_w$:

$$f_w = \frac{u_w}{u}, \quad f_o = \frac{u_o}{u}.$$

Note that $f_w + f_o = 1$. The fractional flow is a really useful quantity, as many models used in waterflooding and polymer flooding adopt a fractional flow formulation. It depends strongly on the saturation of the associated phase. The fractional flow curve has a typical s-shaped form, as it is shown in figure 3.4.

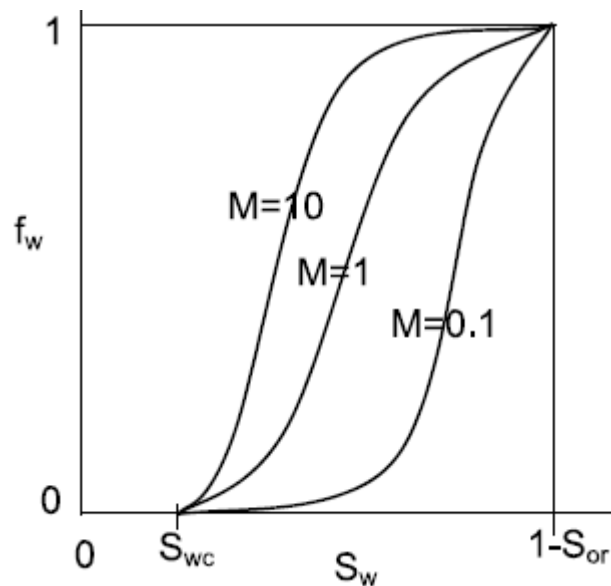
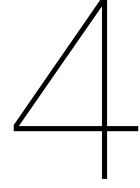


Figure 3.4: Typical curve for water fractional flow f_w with different mobility ratio values. From [8].



Multi-Phase Flow in Porous Media

Before deriving models for polymer flooding and, in particular, for the velocity enhancement effect, it is necessary to present the general and basic equations for fluid flow in porous media. These equations arise from the usual fundamental laws that govern fluid flow, such as conservation of mass, momentum and energy. Through the conservation of mass and employing the empirical Darcy's law, equations for a general flow are derived. Typically, the assumption of incompressibility is made, which is an appropriate approximation far away from the well, where velocities are low. Equations can then be reformulated within the fractional flow theory, resulting in a hyperbolic system of equations. This formulation is also known as the Buckley-Leverett formulation. An analytical solution, characterized by a rarefaction wave and a shock, is then found. Last, Buckley-Leverett theory is extended and addition of polymer to the injected water will be incorporated in the model.

4.1. Mass Conservation

Consider a control volume V with outward normal \mathbf{n} and a general scalar property φ of a one-phase fluid flowing with velocity \mathbf{v} through V . The law of mass balance for the control volume states:

$$\text{rate of inflow} - \text{rate of outflow} = \text{change in mass.}$$

This statement is formulated as

$$\int_{\partial V} -\varphi \mathbf{v} \cdot \mathbf{n} d\partial V = \int_V \frac{\partial \varphi}{\partial t} dV. \quad (4.1)$$

The source term is usually incorporated in the boundary conditions (injection of water-polymer at $x = 0$), therefore it will not be considered here. Using the divergence theorem, (4.1) is rewritten as

$$\int_V \left(\frac{\partial \varphi}{\partial t} + \nabla \cdot (\varphi \mathbf{v}) \right) dV = 0. \quad (4.2)$$

Since the control volume V is arbitrary, the integrand must be equal to zero, namely

$$\frac{\partial \varphi}{\partial t} + \nabla \cdot (\varphi \mathbf{v}) = 0. \quad (4.3)$$

Note that equation (4.3) is a general relation for a conservation of a fluid's property when the source term is absent. For a porous medium, we take $\varphi = \phi\rho$, with ϕ the porosity of the rock and ρ the density of the fluid, and \mathbf{v} is the interstitial velocity. Using the superficial (or Darcy) velocity $\mathbf{u} = \phi\mathbf{v}$, equation (4.3) reads

$$\frac{\partial(\phi\rho)}{\partial t} + \nabla \cdot (\rho\mathbf{u}) = 0. \quad (4.4)$$

For multi-phase flow, the concept of saturation is used. In this case, $\varphi = \phi S_\alpha \rho_\alpha$ and $\mathbf{u}_\alpha = \phi S_\alpha \mathbf{v}_\alpha$, where $\alpha \in \{o, w\}$ denotes the phase considered (oil or water). The equation then reads

$$\frac{\partial(\phi\rho_\alpha S_\alpha)}{\partial t} + \nabla \cdot (\rho_\alpha \mathbf{u}_\alpha) = 0. \quad (4.5)$$

At this point, it is necessary to have an expression for the Darcy's velocities \mathbf{u}_w , \mathbf{u}_o . Darcy's law is an empirical law discovered by Henri Darcy. The differential form of this relation in the case of a single-phase flow is

$$\mathbf{u} = -\frac{k}{\mu} \left(\nabla p + \rho \frac{\mathbf{g}}{g_c} \right), \quad (4.6)$$

where k is the absolute permeability, μ the viscosity, \mathbf{g} the gravitational acceleration vector and g_c some conversion constant. The minus sign is needed because the fluid flows from high pressure to low pressure. If we take the vertical axis z orientated downward, we can write

$$\rho \frac{\mathbf{g}}{g_c} = -\rho \frac{g}{g_c} \nabla z = -\gamma \nabla z,$$

and Darcy's velocity (4.6) can be rewritten as

$$\mathbf{u} = -\frac{k}{\mu} (\nabla p - \gamma \nabla z). \quad (4.7)$$

In the case of multi-phase flow, the definition of Darcy's velocity is slightly modified by introducing the relative permeabilities:

$$\mathbf{u}_\alpha = -\frac{k k_{r,\alpha}}{\mu_\alpha} (\nabla p_\alpha - \gamma_\alpha \nabla z). \quad (4.8)$$

Darcy's velocity (4.8) can be used in the governing equation (4.5) to obtain

$$\frac{\partial(\phi\rho_\alpha S_\alpha)}{\partial t} - \nabla \cdot \left(\rho_\alpha \frac{k k_{r,\alpha}}{\mu_\alpha} (\nabla p_\alpha - \gamma_\alpha \nabla z) \right) = 0, \quad \alpha \in \{w, o\}. \quad (4.9)$$

The system of equations (4.9) has four unknowns, so further relations for the saturations and pressures are needed in order to close the model. From chapter 3, we can use the definitions of saturation and capillary pressure to obtain the following equations:

$$S_w + S_o = 1, \quad (4.10)$$

$$p_c = p_o - p_w. \quad (4.11)$$

The system of differential-algebraic equations (4.9), (4.10) and (4.11) describes the flow of water and oil through a porous medium.

4.2. Fractional Flow Formulation

Classical fractional flow theory was firstly developed by Buckley-Leverett [6, 13] to describe waterflooding. This formulation allows to find an analytical profile for the water saturation. The major assumptions of the model are:

1. Fluids are incompressible.
2. The flow is horizontal and one dimensional.
3. Two phases are flowing.
4. Dispersion is negligible
5. Gravity and capillary forces are negligible.
6. Darcy's law is valid
7. The reservoir is homogeneous.
8. A constant composition is continuously injected, starting at time zero.

If capillarity is negligible, i.e. $p_c = 0$, equation (4.11) yields $p_o = p_w$. Since gravity effect are absent if the flow is horizontal, Darcy's velocities have now the form

$$u_\alpha = \frac{kk_{r,\alpha}}{\mu_\alpha} \frac{\partial p}{\partial x}. \quad (4.12)$$

Due to the incompressibility assumption, equations for the saturation of oil and water read

$$\begin{aligned} \phi \frac{\partial S_w}{\partial t} + \frac{\partial u_w}{\partial x} &= 0, \\ \phi \frac{\partial S_o}{\partial t} + \frac{\partial u_o}{\partial x} &= 0. \end{aligned}$$

Summation of the above equations, along with condition (4.10), yields

$$\frac{\partial u}{\partial x} = 0, \quad (4.13)$$

where $u = u_w + u_o$ is the total (constant) velocity.

The fractional flow coefficients are defined as

$$f_w = \frac{u_w}{u_w + u_o}, \quad f_o = \frac{u_o}{u_w + u_o}, \quad (4.14)$$

Recall that relative permeabilities depend strongly on saturation, so that $f_w = f_w(S_w)$. For the relative permeabilities, Corey's model is employed. Equations using fractional flow coefficients result in

$$\phi \frac{\partial S_w}{\partial t} + u \frac{\partial f_w}{\partial x} = 0, \quad (4.15)$$

$$\phi \frac{\partial S_o}{\partial t} + u \frac{\partial f_o}{\partial x} = 0. \quad (4.16)$$

Typical initial and boundary conditions are

$$\begin{cases} S_w(x, t = 0) = S_{wc}, \\ f_w(x = 0, t) = 1, \end{cases}$$

where S_{wc} is the connate water saturation.

Consider now the classical Buckley-Leverett problem, where continuity equation for water is rewritten as

$$\frac{\partial S_w}{\partial t} + \frac{u}{\phi} \frac{df_w}{dS_w} \frac{\partial S_w}{\partial x} = 0. \quad (4.17)$$

This is a hyperbolic equation for S_w , with characteristic velocity given by

$$\left(\frac{dx}{dt} \right)_{S_w} = \frac{u}{\phi} \frac{df_w}{dS_w}. \quad (4.18)$$

On a front propagating with such velocity, the saturation is constant. However, equation (4.18) cannot be directly integrated because of the s-shaped graph of $f(S_w)$ (see chapter 3). The derivative df/dS_w is not monotone: after a first increasing phase, it starts decreasing in correspondence of the inflection point of $f(S_w)$. Thus, the characteristic lines intersect and, as discussed in chapter 2, a shock forms. The velocity of such shock can be found through an overall material balance on a control volume from the point just behind the shock at time t and just ahead the shock at time $t + \Delta t$ [10]. For the point ahead of the shock, $S_w = S_{wc}$, while for the point behind the shock saturation is denoted by S^* . The material balance gives

$$v_{\Delta S_w} = \frac{u}{\phi} \frac{f_w(S^*) - f_w(S_{wc})}{S^* - S_{wc}}. \quad (4.19)$$

Since the velocities given by (4.18) and (4.19) must be equal at the contact between the shock and the continuous saturation distribution, it holds

$$\frac{f_w(S^*) - f_w(S_{wc})}{S^* - S_{wc}} = \left. \frac{df_w}{dS_w} \right|_{S_w=S^*}. \quad (4.20)$$

For immobile connate water saturation, $f_w(S_{wc}) = 0$, and S^* can be obtained from (4.20) or graphically, since (4.20) is a straight line with slope df_w/dS_w and intercept $(S_{wc}, 0)$, see figure 4.1.

Rewrite equation (4.17) in the conservation form

$$(S_w)_t + f(S_w)_x = 0, \quad (4.21)$$

with $f(S_w) = \frac{u}{\phi} f_w(S_w)$. Along with the initial data

$$S_w(x, 0) = \begin{cases} S_{w,inj} & x < 0, \\ S_{wc} & x \geq 0, \end{cases} \quad (4.22)$$

where $S_{w,inj}$ indicates the saturation of water at the injection point, (4.21) - (4.22) is a Riemann problem for the saturation S_w with flux function $f(S_w)$ as depicted in figure 4.1. Since $S_{w,inj} > S_{wc}$, Theorem 2.2 from chapter 2 states that the solution to (4.21) - (4.22) is found by taking the concave envelope of the flux function. Hence, the straight line in figure 4.1 corresponds to the shock, while the smooth part for $S_w > S^*$ corresponds to the rarefaction wave.

4.3. Polymer Flood

To improve oil recovery, polymer is added to the injected water in order to increase its viscosity, resulting in a more favourable mobility ratio M . The mobility ratio here is defined by

$$M = \frac{\lambda_w}{\lambda_o} = \frac{\mu_o k_{r,w}}{\mu_w k_{r,o}}. \quad (4.23)$$

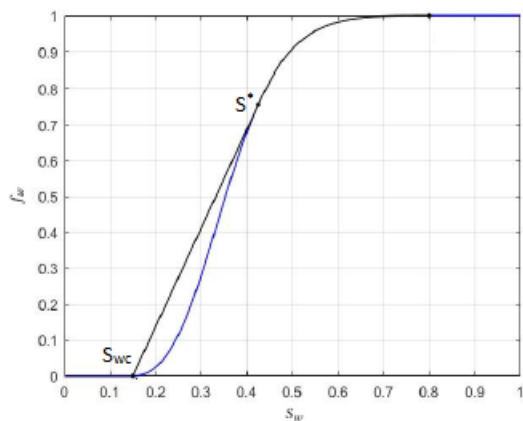


Figure 4.1: Fractional flow function and illustration of an admissible physical solution. From [7].

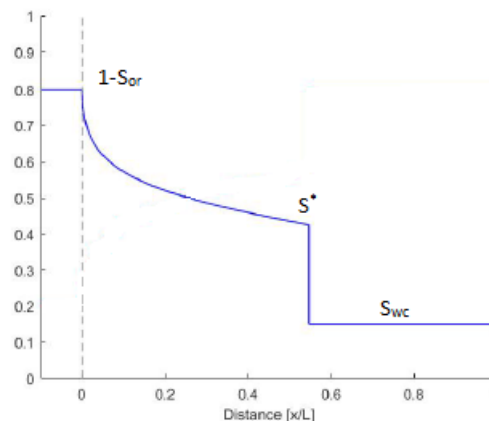


Figure 4.2: Buckley-Leverett solution for a fixed $t > 0$. From [7].

For a water flood, typically $M > 1$. Adding polymer to the injected water will usually lower the mobility ratio to values close to 1. A thorough discussion on polymer flooding can be found in [6, 8].

Since the polymer does not change the residual oil saturation, both waterflooding and polymer flooding will theoretically produce all of the moveable oil over a very long time scale. This time scale, however, is usually many times the practical reservoir development period. The polymer will essentially speed up the recovery, see figure 4.3. The figure shows also an approximated economic limit for both water and polymer flood. Polymer flooding will be particularly useful in those reservoirs where waterflooding is or is predicted to be inefficient. In order to evaluate projects, it is important to predict recovery profiles for waterflood and polymer flood employing different chemical agents. The only way of obtaining these data is to perform different simulations of the proposed projects. This motivates the development and analysis of mathematical models for polymer flood. Although there are many physical and chemical effects that influence the flow of the polymer-water solution through the reservoir, simulations of these models are a good and efficient mean to evaluate proposed projects. Under reasonable assumptions, models for the flow through the reservoir are derived, giving the chance to simulate saturation profiles for injected water and polymer.

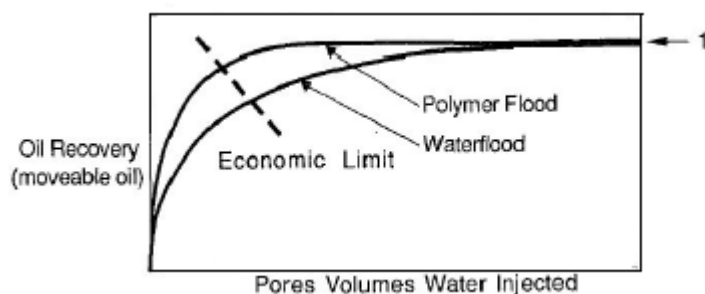


Figure 4.3: Comparison of production profiles for a water flood and a polymer flood. From [6].

4.3.1. Thick Water Model

A first simple approach is to apply classical Buckley-Leverett theory to polymer flooding [2]. This means that the polymer flood is treated as a water flood, only with a different value for viscosity. This model is called the thick water model. Thus, this model is mathematically equivalent to the Buckley-Leverett waterflooding and no new features must be discussed. Figure 4.4 shows two saturation profiles for different mobility ratio: $M = 30$ corresponds to a waterflooding; $M = 1$ corresponds to a polymer flooding. Figure 4.5 shows the recovery for the two cases. As it can be seen, the polymer delays the breakthrough of the water front. As a consequence, even if the ultimate recovery will be the same for both cases, a higher oil recovery will be reached earlier when employing a polymer flooding instead of a waterflooding.

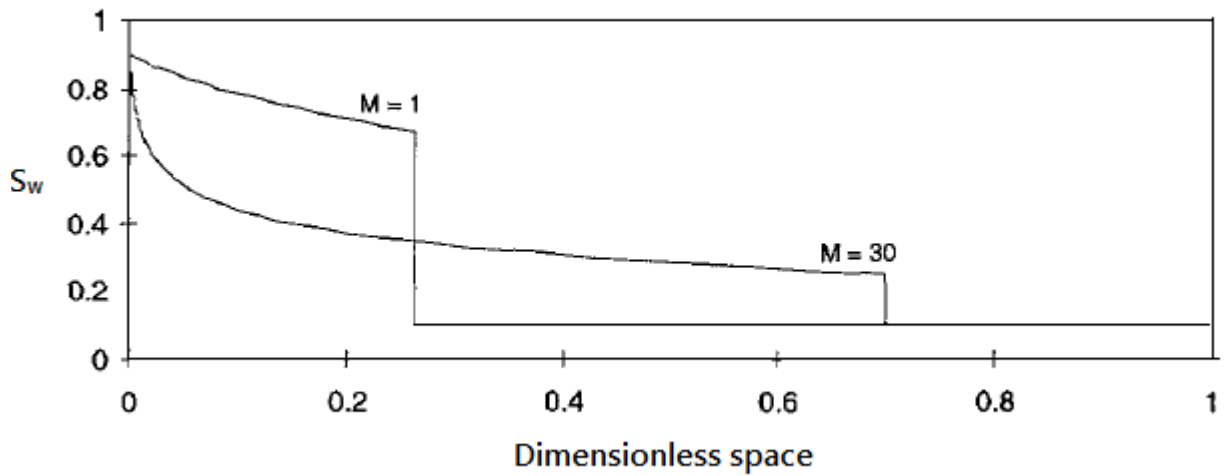


Figure 4.4: Buckley-Leverett front for water flood ($M = 30$) and polymer flood with thick water model ($M = 1$). From [2].

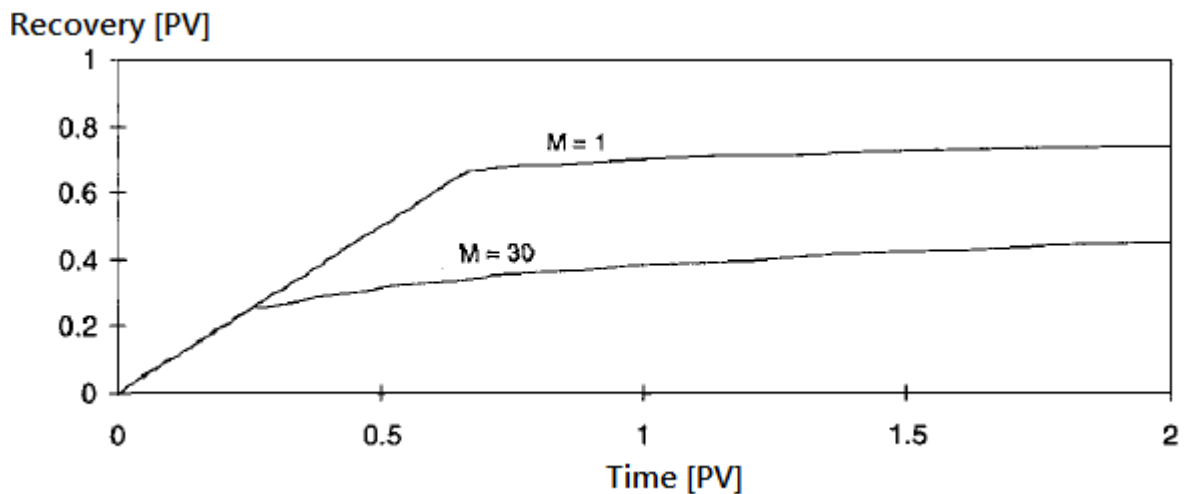


Figure 4.5: Recovery for water flood ($M = 30$) and polymer flood with thick water model ($M = 1$) [2].

4.3.2. Extended Fractional Flow Theory

To have a more accurate model, classical Buckley-Leverett fractional flow theory can be extended [6, 10], deriving a continuity equation also for the polymer concentration c . On top of the assumptions stated above for the fractional flow theory for waterflooding, further assumptions for the polymer are

1. The polymer solution has a Newtonian flow behaviour.
2. Polymer dispersion, gravity, capillary forces and adsorption to rock are negligible.
3. The polymer is present only in the aqueous phase.

The purpose of this section is to derive a qualitative profile for the water saturation and polymer concentration, therefore we disregard effects that would lead to unnecessary complexities. Several assumptions can be weakened easily.

Since the polymer influences the water viscosity, and thus the mobility, the fractional flow function depends not only on the water saturation, but also on the polymer concentration. When adding polymer to water, the fractional flow curve shifts toward the right, as shown in figure 4.6.

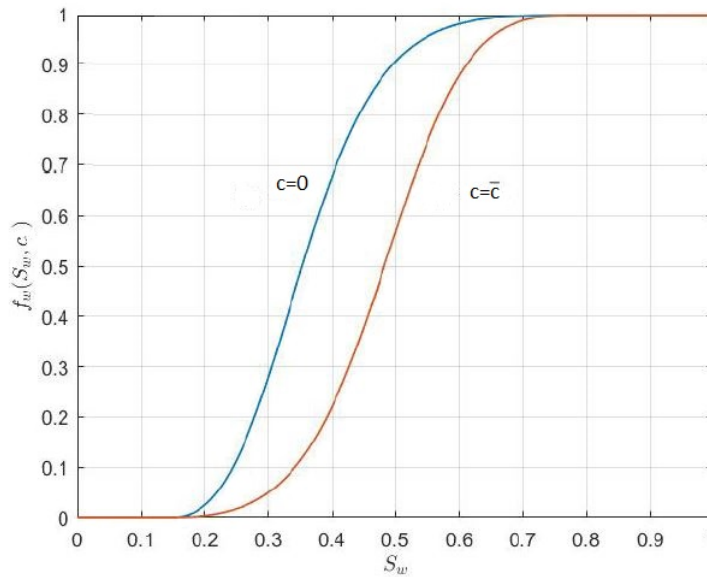


Figure 4.6: Fractional flow functions for pure water (blue line) and water with polymer (red line) [7].

According to Pope [10], continuity equations for water and polymer in fractional flow formulation are

$$\phi \frac{\partial S_w}{\partial t} + u_T \frac{\partial (f_w(S_w, c))}{\partial x} = 0, \quad (4.24)$$

$$\phi \frac{\partial (S_w c)}{\partial t} + u_T \frac{\partial (c f_w(S_w, c))}{\partial x} = 0. \quad (4.25)$$

The dependence of water viscosity on polymer concentration can be modelled by the Flory-Huggins equation [8]:

$$\mu_w(c) = \mu_w^0 (1 + \alpha_1 c + \alpha_2 c^2 + \alpha_3 c^3) = \mu_w^0 \mu_{mult}(c), \quad (4.26)$$

where μ_w^0 is the water viscosity without polymer, μ_{mult} the viscosity multiplier function and α_i some constants.

To complete equations (4.24) and (4.25), a Riemann initial condition is assigned for both water and polymer:

$$S_w(x, 0) = \begin{cases} S_{w,inj} = 1 - S_{or} & x < 0, \\ S_{w,0} = S_{wc} & x \geq 0, \end{cases} \quad (4.27)$$

$$c(x, 0) = \begin{cases} \bar{c} & x < 0, \\ 0 & x \geq 0. \end{cases} \quad (4.28)$$

During a polymer flood, generally two shocks arise [10]: one at the polymer front, where polymer contacts connate water, and one as the water saturations increases from its initial value (as in the waterflood). To compute the shocks velocities, it is useful to rewrite equation (4.25) for the polymer concentration. Expanding equation (4.25) and using (4.24), the equation for polymer concentration is rewritten as

$$\phi S_w \frac{\partial c}{\partial t} + u_T f_w \frac{\partial c}{\partial x} = 0. \quad (4.29)$$

The characteristic velocities for polymer concentration and water saturation are

$$\left(\frac{dx}{dt} \right)_c = \frac{u f_w}{\phi S_w}, \quad (4.30)$$

$$\left(\frac{dx}{dt} \right)_{S_w} = \frac{u}{\phi} \frac{df_w}{dS_w}. \quad (4.31)$$

Thus, saturation S^{*1} at the polymer front can be found by solving

$$\frac{f_w(S^{*1}, \bar{c})}{S^{*1}} = \frac{df_w}{dS_w}(S^{*1}).$$

The water saturation S^{*2} just in front of the shock is found by comparing jump conditions across the shock:

$$\frac{f_w}{S_w}(S^{*1}) = \frac{f_w(S^{*1}, \bar{c}) - f_w(S^{*2}, 0)}{S^{*1} - S^{*2}}.$$

The water saturation S^{*3} just behind the first water front is equal to that of a standard Buckley-Leverett front:

$$\left(\frac{df_w}{dS_w}(S^{*3}) \right) = \frac{f_w(S^{*3}, 0)}{S^{*3} - S_{wc}}.$$

Two distinct cases are then possible. If $S^{*2} \leq S^{*3}$, then there will be a constant plateau for water saturation between the two shocks (case shown in figure 4.7), which forces $S^{*3} = S^{*2}$. If instead $S^{*2} > S^{*3}$, then, after a smaller plateau, the saturation will decrease from S^{*2} to S^{*3} just behind the water front. Behind the water front, saturation is constant and equal to S_{wc} .

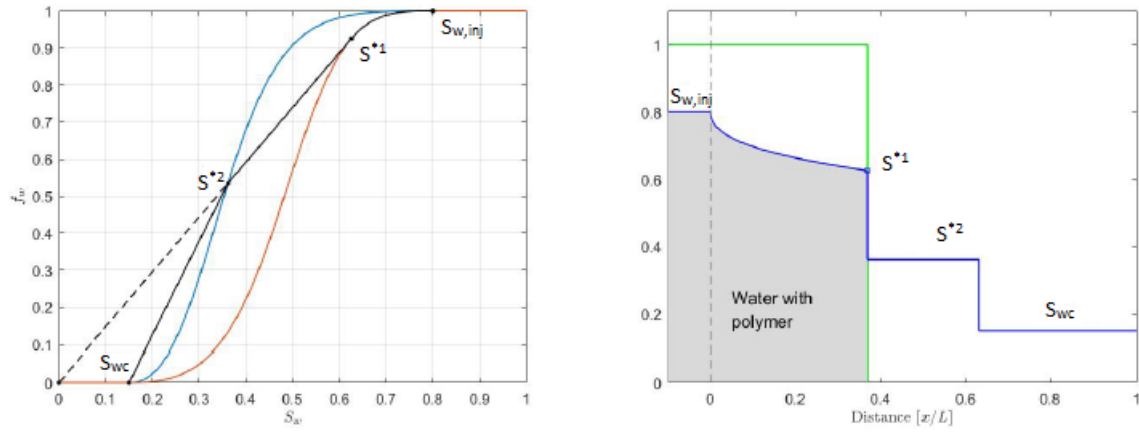


Figure 4.7: Construction of the polymer flooding solution through fractional flow function curve (left); water saturation profile in blue and polymer concentration in green (right). From [7].

5

Velocity Enhancement Models for Polymer Flooding

The models introduced in chapter 4 for polymer flooding are rather qualitative and disregard many physical and chemical properties of rock, fluid and their interaction. Although they are useful to gain insights on the behaviour of the floods, these models should be refined to achieve a more realistic simulation. Modeling further physical phenomena may quickly lead to complexities in the analytical model, requiring numerical methods to be very accurate and computationally efficient. According to Dawson [11], adsorption of polymer molecules onto the rock plays an important role in polymer flooding, causing a delay of the polymer effluent profile. The resulting water bank will be gradually denuded of polymer, depending on the nature of the polymer and reservoir rock. Therefore, adsorption should be included in any realistic mathematical model. However, the effect that will be investigated in this chapter, studied previously for instance by [2, 6, 11], is the velocity enhancement effect due to inaccessible and excluded pore volumes (IPV and EPV, respectively). Since the polymer's molecules have a larger size, they may not access the smallest pores of the rock (IPV) and they may be excluded from the layer close to the wall of the channels (EPV), where velocities are lower. These combined effects result in a velocity enhancement of the polymer's molecules. In some experiments, the polymer is observed to travel faster than the water in which it is dissolved, meaning that IPV and EPV effects overwhelm adsorption and other polymer retention mechanisms. In these cases, the polymer accumulates at the water front. Whether IPV/EPV effects or adsorption dominate the flow depends on the reservoir and polymer properties. In this chapter, models for the velocity enhancement factor will be presented and discussed. It will turn out that this factor causes some mathematical issues, and caution should be exercised in the interpretation of the overall phenomenon and of the simulation results.

5.1. Inaccessible and Excluded Pore Volumes

It was first observed experimentally [11] that polymer molecules are transported through the porous media faster than those of an inert tracer. Dawson et al. named this effect Inaccessible Pore Volumes. The physical interpretation was that the polymer's molecules, due to their larger size, cannot enter the smallest pore of the rock (the ones whose size is smaller than polymer's molecules). Since the polymer moves

through larger pores than an inert tracer, it tends to move ahead, accumulating at the front. The result of the original experiments demonstrating the IPV effect is shown in figure 5.1, where they used polyacrylamide as polymer in a Berea sandstone. The polymer's effluent concentration profile anticipates the one of salt. Dawson and Lantz worked then on several experiments where they managed to combine adsorption and IPV effects, to see how the concentration profile would look depending on which factor is dominating the polymer's flow. Results are illustrated in figure 5.2. They concluded that IPV has a beneficial effect on field performance as it contrasts adsorption, so that polymer response will be seen sooner than expected at production well. In addition, they stated that mathematical models and fields predictions developed without including IPV and adsorption effects will be in error.

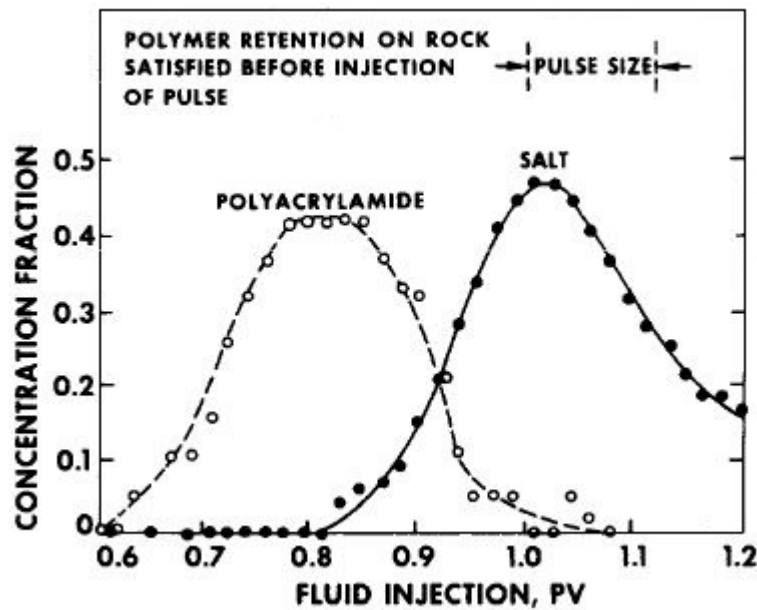


Figure 5.1: Experimental concentration profiles for polymer (polyacrylamide) and salt. From [11].

An alternative physical interpretation of the velocity enhancement effect, known as excluded pore volumes, has been given later (see [2, 6] and literature referenced there). Polymer molecules, once more due to their larger size, are excluded from a layer close to the pore wall. The polymer tends then to travel at the center of the pore throats. Since the streamlines away from the wall are associated with higher velocities, the polymer winds up travelling faster than an inert tracer.

Typically, the magnitude of the velocity enhancement factor is such that the polymer travels at velocities up to about 20% faster than tracer species. When velocity enhancement effects are observed, they may be caused by a combination of IPV and EPV. If the velocity enhancement effect is simply modeled mathematically by a constant factor α , essentially both models presented above are included. A constant velocity enhancement factor may though lead to an unphysical peak of polymer concentration at the water front. Bartelds [3] showed that using a constant α results in an ill-posed problem. Refined model for the factor α are then necessary to get rid of unphysical behaviours. At this point, IPV and EPV may be modeled differently, since they have distinct physical interpretation. Typically, the EPV effect is preponderant over IPV, but it is also more difficult to model. Bartelds proposed a model for the IPV effect using a percolation approach; the same approach is used also in [2] to model

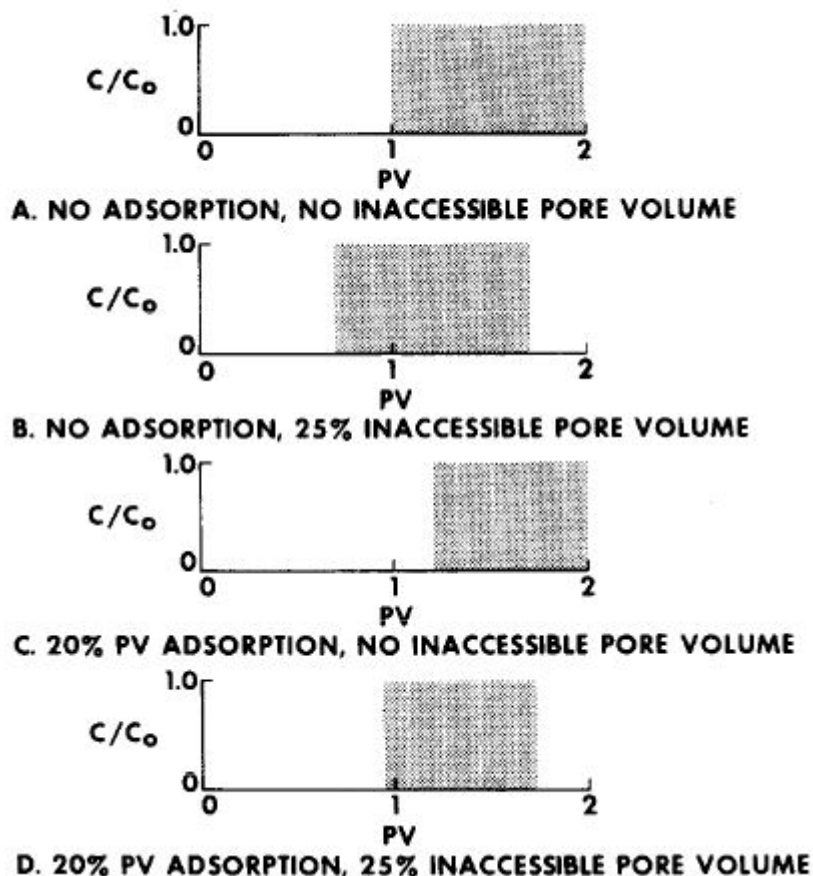


Figure 5.2: Breakout curves for various combination of IPV and adsorption. From [11].

EPV.

Going one step back, it is essential to understand the consequences on the polymer concentration profile of the velocity enhancement. According to Dawson et al. [11], polymer arrives earlier at the effluent than an inert tracer, as shown in figure 5.1. Bartelds model [2] (suited to model EPV) suggests that a peak in polymer concentration should occur in correspondence with the water front (figure 5.3). Several experimental results support this fact, confirming that this is indeed a physical solution and not a mere numerical effect: varying different parameters, such as injection velocity and injection concentration, and using different cores to consider other aspects such as adsorption, core length, permeabilities, etc., a peak in the polymer concentration is measured. Conclusions are that experiments show a significant peak in polymer concentration just after water breakthrough and they are qualitatively in good agreement with simulation results. The balance between retention mechanisms (such as adsorption) and IPV and EPV effects appear to determine the amount of polymer accumulated at the water-oil interface.

5.2. Models for the Velocity Enhancement Factor

Given the influence of IPV and EPV effects on the polymer flood, models for the velocity enhancement factor α are needed in order to perform more realistic simulations. Following the approach of Bartelds [3], the velocity enhancement factor is defined as

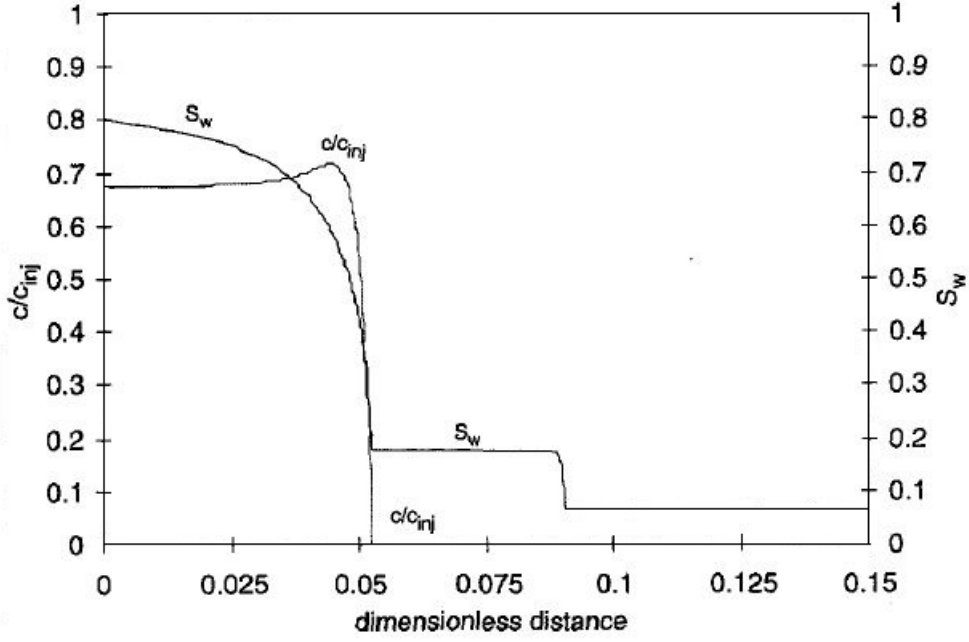


Figure 5.3: Polymer flood simulation: water saturation and polymer concentration profiles for a fixed time. From [2].

the ratio between the average interstitial velocities of polymer and water, namely

$$\alpha = \frac{\langle v_p \rangle}{\langle v_w \rangle}. \quad (5.1)$$

5.2.1. Constant Velocity Enhancement Factor

In first approximation, one may employ a constant value for α . Introducing the effective porosity ϕ_p for the polymer and using Darcy's velocities, (5.1) takes the form

$$\alpha = \frac{v_p}{v_w} = \frac{u_w/\phi_p}{u_w/\phi} = \frac{\phi}{\phi_p}. \quad (5.2)$$

However, in this section results from [3], showing that this choice for α leads to an ill-posed problem when dispersive effects are ignored, will be presented.

In chapter 4, conservation equations for both water and polymer were derived in a fractional flow formulation. Adding to this model an adsorption term and a constant velocity enhancement factor, the governing equations become

$$\phi \frac{\partial S_w}{\partial t} + u \frac{\partial f_w}{\partial x} = 0, \quad (5.3)$$

$$\phi \frac{\partial c S_w}{\partial t} + \phi \frac{\partial a}{\partial t} + \alpha u \frac{\partial c f_w}{\partial x} = 0, \quad (5.4)$$

where $a(c)$ is the concentration of the polymer adsorbed to the rock. Polymer adsorption to the porous media is assumed to be instantaneous and depending on polymer concentration, such that

$$\frac{da}{dc} \geq 0. \quad (5.5)$$

The fractional flow f_w is a function of water saturation and polymer concentration such that

$$\frac{df_w}{dc} < 0, \quad \frac{df_w}{dS_w} \geq 0. \quad (5.6)$$

Multiplying equation (5.3) by c and subtracting it from (5.4), after some manipulations the system of equations can be rewritten in the semi-linear form

$$\frac{\partial}{\partial t} \begin{pmatrix} S_w \\ c \end{pmatrix} + \mathcal{A} \frac{\partial}{\partial x} \begin{pmatrix} S_w \\ c \end{pmatrix} = \begin{pmatrix} 0 \\ 0 \end{pmatrix}, \quad (5.7)$$

where

$$\mathcal{A} = \frac{u}{\phi} \begin{pmatrix} \frac{\partial f_w}{\partial S_w} & \frac{\partial f_w}{\partial c} \\ \frac{(\alpha-1)c \frac{\partial f_w}{\partial S_w}}{S_w + \frac{da}{dc}} & \frac{\alpha f_w + (\alpha-1)c \frac{\partial f_w}{\partial c}}{S_w + \frac{da}{dc}} \end{pmatrix}. \quad (5.8)$$

The nature of the system depends on the eigenvalues of matrix \mathcal{A} : if the eigenvalues are real for all values of S_w and c , then system (5.7) is hyperbolic; if the eigenvalues are complex for some values of S_w and c , the system has elliptic regions. The eigenvalues λ are found solving the quadratic equation

$$\det(\mathcal{A} - \lambda I) = 0. \quad (5.9)$$

To have only real solutions, the discriminant D of (5.9) must be nonnegative. The expression for the discriminant is

$$D = \left(\frac{u}{\phi}\right)^2 \left[\left(\frac{\partial f_w}{\partial S_w} - \frac{\alpha f_w + (\alpha-1)c \frac{\partial f_w}{\partial c}}{S_w + \frac{da}{dc}} \right)^2 + 4 \left(\frac{\partial f_w}{\partial c} \frac{(\alpha-1)c \frac{\partial f_w}{\partial S_w}}{S_w + \frac{da}{dc}} \right) \right]. \quad (5.10)$$

First, consider the case where $\alpha = 1$ (no velocity enhancement effect). As discussed within the fractional flow theory in chapter 4, at the polymer front the saturation is found by equating the velocities of the water saturation front and polymer concentration front, giving

$$\frac{\partial f_w}{\partial S_w} = \frac{f_w}{S_w + \frac{da}{dc}}. \quad (5.11)$$

Since it is reasonable to assume that ill-posedness of the model would cause problems at the shock, we study expression (5.10) for the discriminant when (5.11) holds. In the case of $\alpha = 1$, this assumption implies that $D = 0$, thus the eigenvalues are real (and equal) and the system is hyperbolic. To analyze the discriminant for $\alpha > 1$, define the region H to be the set of all pairs (S_w, c) where the two eigenvalues are equal for $\alpha = 1$, i.e. where (5.11) holds:

$$H = \left\{ (S_w, c) \left| \frac{\partial f_w}{\partial S_w} = \frac{f_w}{S_w + \frac{da}{dc}} \right. \right\}. \quad (5.12)$$

Setting $\alpha = 1 + \epsilon$, for $(S_w, c) \in H$ the expression for the discriminant is

$$D = \left(\frac{u}{\phi}\right)^2 \left[\frac{\epsilon}{S_w + \frac{da}{dc}} \left(\frac{\epsilon}{S_w + \frac{da}{dc}} \left(c \frac{\partial f_w}{\partial c} + f_w \right) + 4c \frac{\partial f_w}{\partial c} \frac{\partial f_w}{\partial S_w} \right) \right]. \quad (5.13)$$

Since ϵ may be chosen arbitrarily small, the term on the right of (5.13) dominates and, due to (5.6), the discriminant is negative. This means that the eigenvalues are complex and there exists an elliptic region around the set H : the model is ill-posed.

The presence of an elliptic region leads to instabilities in the numerical solutions. Using a Corey model for the relative permeabilities and a velocity enhancement factor $\alpha = 1.1$, results shown in figure 5.4 are obtained. Just before the shock, there is an unbounded peak in the polymer concentration. The height of the peak depends on the mesh of the grid, giving an indication of the ill-posed behaviour of the system. The plot in the phase space shows that the peak in the polymer concentration occurs when the solution crosses the elliptic region. Note that the initial condition $(S_w, c) = (S_{wc}, 0)$ and the injection condition $(S_w, c) = (1 - S_{or}, c_i)$ are separated by the elliptic regions, which therefore has to be crossed by the solution.

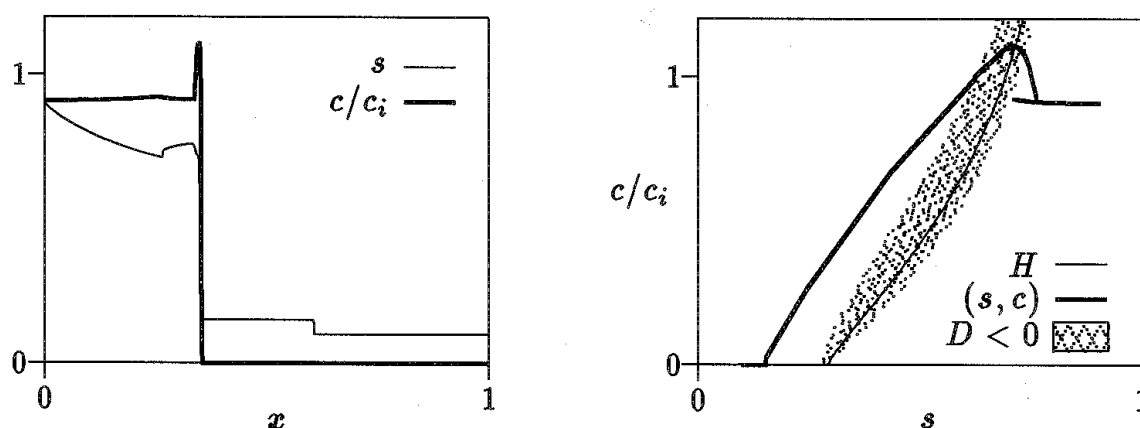


Figure 5.4: Numerical solutions of saturation and concentration in x -space (left) and in phase-space (right) at $t = 0.25$ PV injected and $\alpha = 1.1$. From [3].

5.2.2. Percolation Model

In order to improve the model and get rid of instabilities, Bartelds [3] proposed a model of the velocity enhancement factor based on percolation theory. Percolation theory describes through statistical means the morphology of, and transport through, randomly disordered media. We restrict now exclusively to the IPV effect, because it is easier to model using this approach. Extension to EPV effect is studied by Bartelds in [2].

To use a percolation-type description, the polymer flood is seen as a three-phase flow. These phases are:

1. Water which cannot contain polymer, with saturation denoted by S_{w1} .
2. Water which may potentially contain polymer, with saturation denoted by S_{w2} .
3. Oil without polymer, with saturation S_o .

Polymer is restricted to water phase 2, while exchange of water molecules between phase 1 and 2 is allowed. It is assumed further that there is local equilibrium in the polymer concentration, meaning that there is instantaneous diffusion of polymer molecules between movable water and the part of connate water which is accessible to polymer.

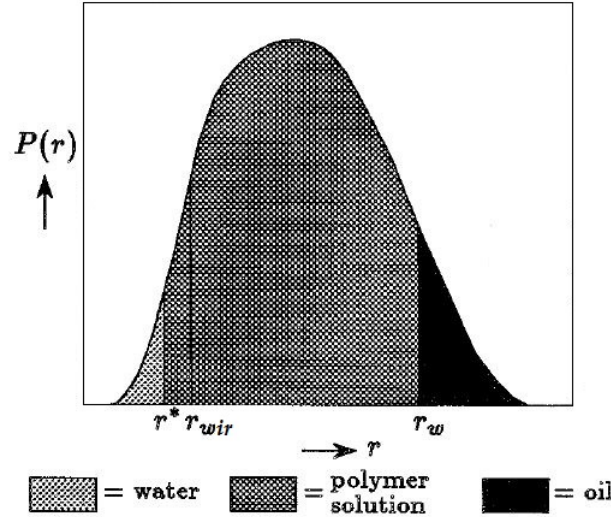


Figure 5.5: Example of a probability distribution showing the threshold radius and the three different phases. From [3].

Percolation theory is used to model networks that consist of branches and nodes. The accessible bonds of the network are the one that are actually under study because they fulfill a specific requirement or condition. The basic idea used to apply a percolation approach is that the smallest pores do not contain polymer molecules (IPV), thus polymer is excluded from the pores with radius smaller than a threshold value r^* . The accessible bonds in the model are then the pore throats with $r > r^*$. Figure 5.5 illustrates an example of a probability density function $P(r)$ describing the distribution of pores radii. This probability density function gives the fractional volume occupied by pores with radius belonging to some interval.

In water-wet media, water prefers to enter pores in a sequence of increasing radius. This means that all the pores with $r < r^*$ have to be filled with water before polymer is allowed to enter the porous media. The threshold water saturation needed to fulfill this condition is denoted by S^* and it is assumed to be lower than the irreducible water saturation, i.e. $S^* < S_{wir}^1$. The water phase 1 where polymer is not allowed corresponds then to the area of $P(r)$ with $r < r^*$. The associated saturation is $S_{w1} = S^*$. The water phase 2 correspond to the area where $r^* < r < r_w$, and its saturation is $S_{w2} = S_w - S^*$.

Model equations for the three phase flow read

$$\phi \frac{\partial S_{w1}}{\partial t} + \frac{\partial u_{w1}}{\partial x} = R, \quad (5.14)$$

$$\phi \frac{\partial S_{w2}}{\partial t} + \frac{\partial u_{w2}}{\partial x} = -R, \quad (5.15)$$

$$\phi \frac{\partial c_{w2} S_{w2}}{\partial t} + \phi \frac{\partial a}{\partial t} + \frac{\partial c_{w2} u_{w2}}{\partial x} = 0, \quad (5.16)$$

where R denotes the net transfer rate of water molecules from phase 1 to phase 2. It is convenient to introduce the average polymer concentration c in the total water

¹The assumption of Bartelds is actually $S^* < S_{wc}$, but it is also assumed that the connate water is immobile. This fact was noticed by Hilden et al. [14], who then concluded that in Bartelds [3] $S_{wc} = S_{wir}$. For the purpose of comparison, here we use the irreducible water saturation.

phase,

$$c = \frac{c_{w2}S_{w2}}{S_{w1} + S_{w2}}. \quad (5.17)$$

The adsorption term a is assumed to be function only of this average concentration.

The velocity enhancement factor can be expressed as

$$\alpha = \frac{v_p}{v_w} = \frac{v_{w2}}{v_w} = \frac{u_{w2} S_w}{S_{w2} u_w} = \frac{u_{w2}}{u_{w1} + u_{w2}} \frac{S_{w1} + S_{w2}}{S_{w2}}. \quad (5.18)$$

Since it assumed that $S_{w1} = S^* < S_{wir}$, $\partial S_{w1}/\partial t$ is zero and water phase 1 is unable to flow, giving $u_{w1} = 0$. It follows that the transfer rate R is zero: no water is exchanged between phase 1 and phase 2. Using $S_{w1} = S^*$ and $S_{w2} = S_w - S^*$ in (5.18), the velocity enhancement factor becomes

$$\alpha(S_w) = \frac{S_w}{S_w - S^*}. \quad (5.19)$$

Thus, in this model, the velocity enhancement factor is no longer constant, but it depends on the water saturation S_w . Typically, near the connate water saturation the factor has higher values, and it decreases to an almost constant value as water saturation increases.

Using (5.19), the average polymer concentration can be written as

$$c = \frac{c_{w2}}{\alpha}. \quad (5.20)$$

Rewriting the conservation equations in fractional flow formulation ($u_w = f_w u$) and using (5.20) and (5.19), the final governing system is

$$\phi \frac{\partial S_w}{\partial t} + u \frac{\partial f_w}{\partial x} = 0, \quad (5.21)$$

$$\phi \frac{\partial a}{\partial t} + \phi \frac{\partial c S_w}{\partial t} + u \frac{\partial \alpha c f_w}{\partial x} = 0. \quad (5.22)$$

To study the well-posedness, the same approach as with the constant velocity enhancement factor is followed. Governing equations are rewritten in the matrix-vector form

$$\frac{\partial}{\partial t} \begin{pmatrix} S_w \\ c \end{pmatrix} + \mathcal{A} \frac{\partial}{\partial x} \begin{pmatrix} S_w \\ c \end{pmatrix}, \quad (5.23)$$

where the matrix \mathcal{A} is given by

$$\mathcal{A} = \frac{u}{\phi} \begin{pmatrix} \frac{\partial f_w}{\partial S_w} & \frac{\partial f_w}{\partial c} \\ \frac{\frac{d\alpha}{dS_w} c f_w + (\alpha-1)c \frac{\partial f_w}{\partial S_w}}{S_w + \frac{da}{dc}} & \frac{\alpha f_w + (\alpha-1)c \frac{\partial f_w}{\partial c}}{S_w + \frac{da}{dc}} \end{pmatrix}. \quad (5.24)$$

Again, the purpose is to show that the eigenvalues of \mathcal{A} are real by analyzing the discriminant of the characteristic equation. Using

$$\frac{d\alpha}{dS_w} = -\frac{\alpha(\alpha-1)}{S_w},$$

after some tedious manipulations the expression for the discriminant takes the form

$$D = \left(\frac{\partial f_w}{\partial S_w} \left(S_w + \frac{da}{dc} \right) + (\alpha-1)c \frac{\partial f_w}{\partial c} - \alpha f_w \right)^2 - 4\alpha(\alpha-1)c f_w \frac{\partial f_w}{\partial c} \frac{da}{dc}. \quad (5.25)$$

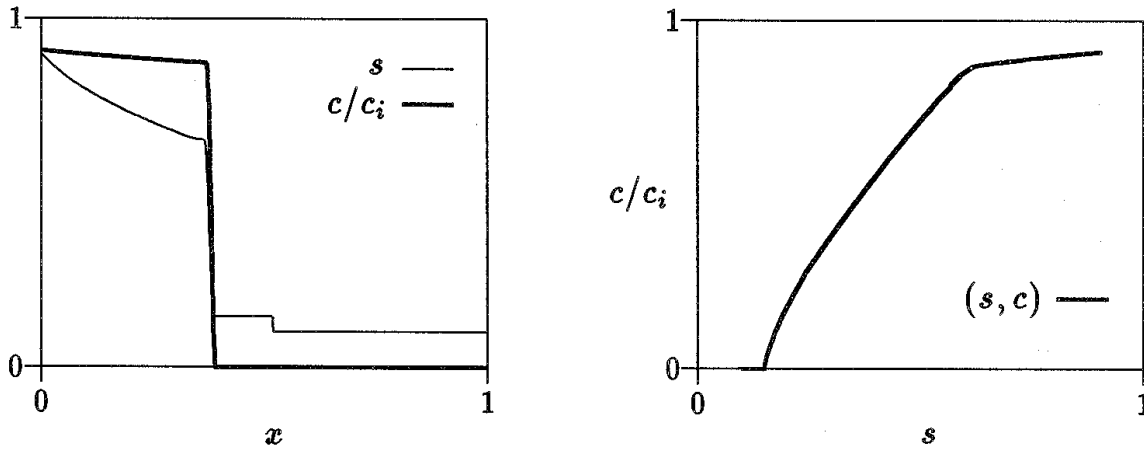


Figure 5.6: Numerical solutions of saturation and concentration in x -space (left) and in phase-space (right) at $t = 0.25$ PV injected for $\alpha = S_w/(S_w - S^*)$. From [3].

From (5.5), (5.6) and the fact that $\alpha(S_w) > 1$, it follows that the discriminant is non-negative and there are no elliptic regions. It must be remarked that this model is valid under the assumption $S^* < S_{wir}$. This restriction is though acceptable since a commonly observed value for α is 1.1, which corresponds to a threshold saturation $S^* = 0.091$. Most reservoirs have a value of irreducible water saturation larger than 0.1, so that assuming $S^* < S_{wir}$ is reasonable.

Using the same test problem of the previous section, where a constant velocity enhancement factor caused a peak in the concentration at the polymer front, results shown in figure 5.6. The peak now is absent and there is no polymer accumulation at the front.

In conclusion, a constant velocity enhancement factor leads to an ill-posed model that causes an unphysical pile-up of the polymer at the polymer front, disregarding any retardation effect such as adsorption. The height of the peak is unbounded and depends on the grid spacing used in the simulation. Moreover, the constant velocity factor model does not have a clear physical counterpart and it is just a convenient mathematical model. The saturation-dependent model for the velocity enhancement factor presented by Bartelds is built on a clear physical concept and the resulting equations are shown to be well-posed (without elliptic regions), so that numerical instabilities are not an issue. The model proposed takes into consideration only IPV effects. Other mechanisms, such as EPV, may though lead to a physical pile-up of the polymer. However, this pile-up should not depend on the numerical mesh and grow unbounded as with the constant velocity enhancement factor.

The percolation model has been extended by Bartelds to consider the EPV effect as the major cause of velocity enhancement. The conservation equations are still (5.21) and (5.22), while the velocity enhancement factor is expressed as

$$\alpha(S_w) = \frac{S_w k_{r,w2}}{S_{w2} k_{r,w}}. \quad (5.26)$$

The relative permeabilities $k_{r,w}$ and $k_{r,w2}$ are determined using a percolation approach. For a detailed discussion of this model, the reader is referred to [2]. The main result that must be outlined is that this model allows for accumulation of polymer at the front, as it was shown in section 5.1, figure 5.3. The profile obtained

was qualitatively in good agreement with the physical experiments, confirming that a pile-up of the polymer may actually occur. Caution must then be exercised when interpreting simulation results, since the polymer pile-up may arise from numerical stability issues or instead be the correct physical profile.

5.2.3. Hilden-Nilsen-Raynaud Model

The models proposed by Bartelds for IPV seeks and succeeds in solving stability issues related to the velocity enhancement factor modeling. Numerical solutions are smooth and no peaks in polymer concentration appears to grow unbounded. The model is though subject to the restriction $S^* < S_{wir}$, where S^* is some threshold saturation that must be reached by water before polymer is allowed to be transported through the porous medium. Since it is not guaranteed that this condition holds for every reservoir, Hilden et al. [14] proposed an extended model to relax this assumption. Based on an heuristic physical understanding of the relative permeabilities, an alternative model is derived. This model reduces to the one proposed by Bartelds when the inaccessible pore volume is smaller than the irreducible water saturation, which is basically the assumption $S^* < S_{wir}$. Considering shock solutions, a necessary condition that must be fulfilled by the model in order to be well-posed is derived.

A two-phase water oil flow is considered, where in addition polymer can be part of the water phase. The conservation equations in two dimensions without IPV effects and adsorption are

$$\frac{\partial}{\partial t}(\rho_\alpha \phi S_\alpha) + \nabla \cdot (\rho_\alpha \mathbf{u}_\alpha) = 0, \quad \alpha \in \{o, w\} \quad (5.27)$$

$$\frac{\partial}{\partial t}(\rho_w \phi S_w c) + \nabla \cdot (c \rho_w \mathbf{u}_{wp}) = 0, \quad (5.28)$$

where ρ_α are the phase densities, c the polymer concentration and \mathbf{u}_α , \mathbf{u}_{wp} the Darcy's velocities given by

$$\mathbf{u}_o = - \frac{k_{r,o}}{\mu_o} (\nabla p - \rho_o g \nabla z), \quad (5.29)$$

$$\mathbf{u}_w = - \frac{k_{r,w}}{\mu_{w,eff}} (\nabla p - \rho_w g \nabla z), \quad (5.30)$$

$$\mathbf{u}_{wp} = - \frac{k_{r,wp}}{\mu_{p,eff}} (\nabla p - \rho_w g \nabla z). \quad (5.31)$$

Here, it is assumed that the presence of polymer does not influence oil phase, pressures, densities and relative permeabilities. For the viscosity effect, a Todd-Longstaff [9] model is used. That is, denote the viscosity of a fully mixed water and polymer solution by $\mu_m(c)$, with $\mu_p = \mu_m(c_{\max})$ and c_{\max} the maximum injection concentration of polymer. The effective polymer viscosity is

$$\mu_{p,eff} = \mu_m(c)^\omega \mu_p^{1-\omega},$$

where $\omega \in [0, 1]$ is referred to as the mixing parameter. The viscosity of the partially mixed water is given by

$$\mu_{w,e} = \mu_m(c)^\omega \mu_w^{1-\omega}.$$

The effective water viscosity is defined to be

$$\frac{1}{\mu_{w,eff}} = \frac{1 - c/c_{\max}}{\mu_{w,e}} + \frac{c/c_{\max}}{\mu_{p,eff}}.$$

The velocity enhancement factor $\alpha(S_w)$ can be incorporated in equation (5.28), giving

$$\frac{\partial}{\partial t}(\rho_w \phi S_w c) + \nabla \cdot (\alpha(S_w) c \rho_w \mathbf{u}_{wp}) = 0. \quad (5.32)$$

To derive a necessary condition to ensure well-posedness, conservation equations for water and polymer are rewritten in a one-dimensional fractional flow formulation. Therefore, gravitational effect are not present and incompressibility must be assumed. In addition, the polymer is considered to behave as an inert component, so that water flow is not affected by polymer presence. The resulting equations are

$$\frac{\partial S_w}{\partial t} + \frac{u}{\phi} \frac{\partial f_w(S_w)}{\partial x} = 0, \quad (5.33)$$

$$\frac{\partial(S_w c)}{\partial t} + \frac{u}{\phi} \frac{\partial}{\partial x} (c \alpha(S_w) f_w(S_w)) = 0, \quad (5.34)$$

where $u = u_w + u_o$ is the total velocity. Without loss of generality, assume $u/\phi = 1$. Let $z = S_w c$ and consider the Riemann problem with values (S_l, z_l) and (S_r, z_r) on the left- and right-hand side, respectively. Assume further that solution to (5.33) is a pure shock and that $S_l > S_r$, which is usually the case since, on the left, water is injected and, on the right, we have the connate (or irreducible) water saturation S_{wc} . Such a pair of saturation will be addressed as a single shock pair. Rankine-Hugoniot condition gives the velocity v of the shock

$$v = \frac{f_w(S_l) - f_w(S_r)}{S_l - S_r}. \quad (5.35)$$

Rewrite the polymer equation in a moving frame with velocity v using the coordinate $\hat{x} = x - vt$. After a change of variables, (5.34) becomes

$$\frac{\partial \hat{z}}{\partial t} + \frac{\partial}{\partial \hat{x}} \left(\hat{z} \left(\frac{\alpha(\hat{S}_w)}{\hat{S}_w} f(\hat{S}_w) - v \right) \right) = 0. \quad (5.36)$$

Because of the discontinuity in the water saturation, (5.36) has a discontinuous flux. Removing the hat to simplify the notation, the Riemann problem is

$$\begin{cases} \frac{\partial z}{\partial t} + \frac{\partial(g_l z)}{\partial x} = 0 & \text{if } x < 0, \\ \frac{\partial z}{\partial t} + \frac{\partial(g_r z)}{\partial x} = 0 & \text{if } x > 0, \end{cases} \quad (5.37)$$

where

$$\begin{cases} g_l = \frac{\alpha(S_l) f_w(S_l)}{S_l} - v, \\ g_r = \frac{\alpha(S_r) f_w(S_r)}{S_r} - v. \end{cases} \quad (5.38)$$

Note that the values g_l, g_r are constants. The analysis carried out in section 2.3 for Riemann problems with discontinuous flux function can be used now. A solution to problem (5.37) is formed by gluing together the solutions of two Riemann problems (see section 2.3.1). At the discontinuity, a pair of values z_- and z_+ (which are part of the initial data of the two Riemann problems) must be determined such that the following conditions are fulfilled:

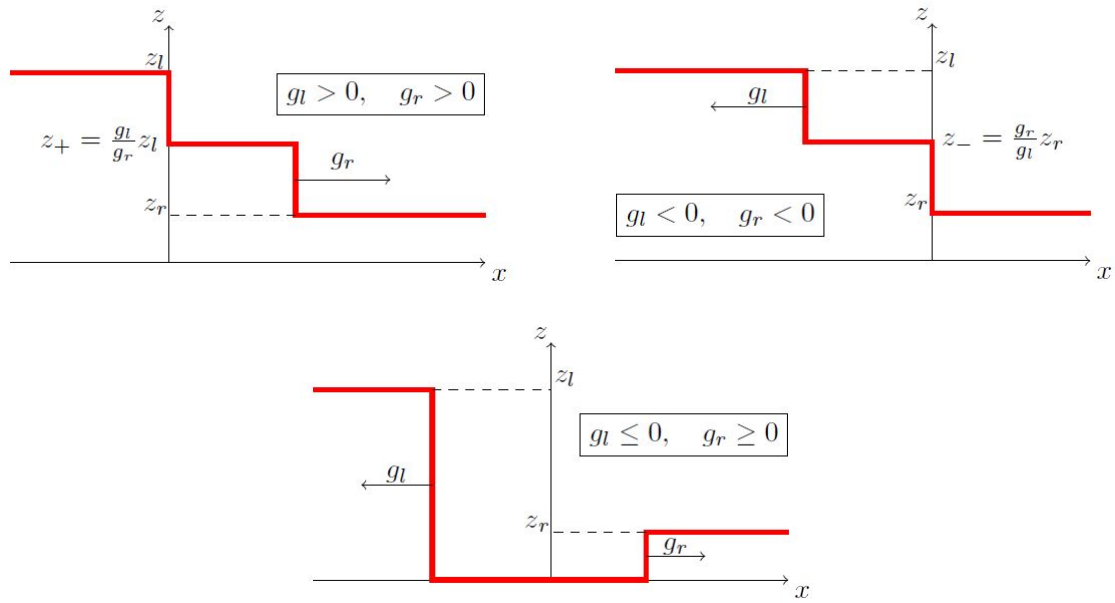


Figure 5.8: Acceptable shock solutions for different signs of g_l and g_r [14].

1. For $x < 0$, there exists a solution to the first equation in (5.37) with only waves traveling from right to left.
2. The jump at $x = 0$ is a discontinuity with zero speed, so the Rankine Hugoniot condition gives $g_l z_- = g_r z_+$.
3. For $x > 0$, there exists a solution to the second equation in (5.37) with only waves traveling from left to right.

If for a pair (z_l, z_r) values for z_- and z_+ are found such that these requirements are satisfied, (z_l, z_r) is called solvable and the Riemann solution joining z_l to z_r is called acceptable. Essentially, to obtain a well-posed problem, the velocity enhancement function $\alpha(S_w)$ must be chosen such that any (nonnegative) pair (z_l, z_r) will be always solvable.

For the three cases presented in figure 5.8, any pair (z_l, z_r) is solvable. For the remaining case

$$g_l \geq 0 \quad \text{and} \quad g_r \leq 0, \quad \text{with} \quad g_l \neq g_r, \quad (5.39)$$

Rankine-Hugoniot condition $g_l z_- = g_r z_+$ implies that either $z_l = z_- = 0$ or $z_r = z_+ = 0$ must hold, but $z = S_w c_p > 0$, so the velocity enhancement factor must be chosen such that (5.39) never occurs. If $S_r = S_{wir}$ (the irreducible water saturation), then $f_w(S_r) = 0$ and (5.38) gives $g_r = -v \leq 0$. Therefore, to ensure that (5.39) does not occur, it must be $g_l \leq 0$. The shock velocity v given by (5.35) is

$$v = \frac{f_w(S_l)}{S_l - S_{wir}}.$$

Using this expression, the condition $g_l \leq 0$ is rewritten as

$$\alpha(S_w) \leq \frac{S_w}{S_w - S_{wir}}, \quad (5.40)$$

for $S_w = S_l$. Inequality (5.40) is a necessary condition for well-posedness of the Riemann problem. Note that, in the model derived by Bartelds, the velocity enhancement factor is

$$\alpha(S_w) = \frac{S_w}{S_w - S^*}. \quad (5.41)$$

In the case $S^* < S_{wir}$ (which is the restriction imposed by Bartelds model), the necessary condition for the factor (5.41) is satisfied. On the other hand, if $S^* \geq S_{wir}$, (5.40) does not hold and the resulting model is ill-posed.

Under mild assumptions on the fractional flow function, it can be shown that condition (5.40) is also sufficient in the sense that, if it is satisfied by any shock pair, then any pair (z_l, z_r) is solvable.

The purpose is then to derive a model satisfying the necessary condition (5.40). The main ideas behind the model proposed by Hilden et al. [14] will be presented. For a thorough and detailed discussion, the reader is referred to the original paper. The assumption that will guide the model's derivation is that, in a water wet system, water invades smallest pores first. In these smallest pores, permeability is lower and water travels slower. Moreover, the flow is assumed to be one-dimensional and incompressible.

Similarly to the percolation model, a distribution function $\chi(\hat{r})$ is defined, where \hat{r} denotes the characteristic radius of a pore. Since permeability is assumed to depend on the pore size, for each \hat{r} there corresponds a permeability $\hat{k}(\hat{r})$ and the total permeability is given by

$$k = n \int_0^\infty \hat{\phi}(\hat{r}) \hat{k}(\hat{r}) \chi(\hat{r}) d\hat{r}, \quad (5.42)$$

where n is the number of pores in a cross section and the function $\hat{\phi}$ contains the geometric information on the structure of this section.

Due to the assumption that pores are filled successively in increasing size, for a given global saturation S_w there exists a threshold value for the pore size, denoted by $r(S_w)$ or simply r , for which

$$\hat{S}_w(\hat{r}) = \begin{cases} 1 & \text{if } \hat{r} \leq r(S_w), \\ 0 & \text{if } \hat{r} > r(S_w). \end{cases} \quad (5.43)$$

The global water saturation is then defined similarly to (5.42) as

$$S_w = \frac{n}{\phi} \int_0^r \hat{\phi}(\hat{r}) \chi(\hat{r}) d\hat{r}, \quad (5.44)$$

Polymer is then included in the model. The inaccessible pore volume effect is modeled by defining a threshold value r^{*2} such that polymer cannot enter pores with $r < r^*$. Polymer concentration can then be expressed as

$$\hat{c}(\hat{r}) = \begin{cases} 0 & \text{if } \hat{r} \leq r^*, \\ \bar{c} & \text{if } \hat{r} > r^*, \end{cases} \quad (5.45)$$

²The threshold values r^* and S^* are actually denoted by Hilden et al. as r_{ipv} and $S_{w,ipv}$, respectively. Since these values are assumed to be equal to the Bartelds' threshold values, we keep the star notation for comparison purposes.

where it is assumed that in the region $\hat{r} > r^*$ the polymer diffuses uniformly and reaches a constant concentration \bar{c} . An expression for the total polymer concentration is then given by

$$S_w c = \frac{n}{\phi} \bar{c} \int_{r^*}^r \hat{\phi}(\hat{r}) \chi(\hat{r}) d\hat{r}. \quad (5.46)$$

These expressions for permeability, saturation and concentration are inserted into the governing equations. An analytical expression for the velocity enhancement factor is found manipulating the system of equations, resulting in

$$\alpha(S_w) = \frac{S_w}{k_{r,w}(S_w)} \frac{k_{r,w}(S_w) - k_{r,w}(S^*)}{S_w - S^*}, \quad (5.47)$$

where $S^* = S_w(r^*)$. To have a well-defined expression, $\alpha(S_w)$ is defined to be zero for $S_w < S^*$. If the function $k_{r,w}(S_w)$ is convex, which is a common feature for relative permeabilities, then the necessary condition (5.40) does not hold for $S^* > S_{wir}$ and the model is still ill-posed. The assumption stated by Bartelds has not been relaxed yet. The idea is then to introduce a weighting function $\hat{w}(\hat{r})$, defined to be equal to zero for $\hat{r} \leq r^*$, since the uniform polymer diffusion assumption may not be appropriate. The polymer concentration (5.45) becomes

$$\hat{c}(\hat{r}) = \hat{w}(\hat{r}) \bar{c}. \quad (5.48)$$

Define the function $W(S_w)$ to be

$$W(S_w) = \frac{n}{\phi} \int_0^r \hat{w}(\hat{r}) \hat{\phi}(\hat{r}) \chi(\hat{r}) d\hat{r}. \quad (5.49)$$

This function is useful since [14]

$$\frac{dW(S_w)}{dS_w} = \hat{w}(\hat{r}), \quad (5.50)$$

so it can be used to define the weighting factor $\hat{w}(\hat{c})$ and it has the form of the other physical properties. If the polymer does not have a preference to invade first regions with larger or smaller pore size, hence it diffuses uniformly, the function $W(S_w)$ will have the expression

$$W(S_w) = \begin{cases} 0 & \text{if } S_w < S^* \\ A(S_w - S^*) & \text{if } S^* < S_w < 1 - S_{or}, \end{cases} \quad (5.51)$$

where A is some constant that can be chosen to be equal to 1 after normalization. It was though shown previously that a uniform polymer diffusion does not lead to a well-posed problem. In an attempt to obtain a well-posed model without renouncing to use a (simpler) uniform polymer diffusion, the definition of inaccessible pore volume can be relaxed by allowing a small quantity of polymer to enter the smallest pores. Thus, $W(S_w)$ is defined as

$$W(S_w) = \begin{cases} \frac{\epsilon}{S^*} S_w & \text{if } S_w < S^* \\ \epsilon + (S_w - S^*) & \text{if } S^* < S_w < 1 - S_{or}. \end{cases} \quad (5.52)$$

For $\epsilon \rightarrow 0$, (5.52) reduces to (5.51). Technically, the polymer diffusion is non-uniform if definition (5.52) is employed for $W(S_w)$. Indeed, the diffusion will change depending

whether the water saturation is greater or smaller than the inaccessible pore volume saturation S^* . If $S^* < S_{wir}$, (5.52) is simply $W(S_w) = \epsilon + S_w - S_{w,ipv}$, and the necessary condition is fulfilled $\forall \epsilon \geq 0$, in particular for $\epsilon = 0$. For this choice of ϵ , the velocity enhancement factor reduces to the one obtained by Bartelds, namely

$$\alpha(S_w) = \frac{S_w}{S_w - S^*}.$$

It is more challenging to analyze the case $S^* > S_{wir}$, which so far has lead to ill-posedness for all the proposed models. The expression for the velocity enhancement factor in this case is

$$\alpha(S_w) = \begin{cases} 1 & \text{if } S_w \leq S^* \\ S_w \frac{k_{r,w}(S_w) + \frac{\epsilon - S^*}{S^*} k_{r,w}(S^*)}{(S_w + \epsilon - S^*) k_{r,w}(S^*)} & \text{if } S_w > S^*. \end{cases} \quad (5.53)$$

The necessary condition is satisfied for $S_w \leq S^*$, since it always holds $1 < \frac{S_w}{S_w - S_{wir}}$. For the remaining case $S_w > S^*$, adopt the Corey's model for the water relative permeability, which is recalled to be

$$k_{r,w} = \left(\frac{S_w - S_{wir}}{1 - S_{wir} - S_{ot}} \right)^{N_w},$$

with $N_w \geq 1$. The necessary condition for well-posedness forces

$$\frac{k_{r,w}(S_w) + \frac{\epsilon - S^*}{S^*} k_{r,w}(S^*)}{(S_w + \epsilon - S^*) k_{r,w}(S^*)} \leq \frac{1}{S_w - S_{wir}}, \quad (5.54)$$

which may be reformulated requiring that the function $F(S_w, \epsilon)$, defined as

$$F(S_w, \epsilon) = (S_w + \epsilon - S^*)(S_w - S_{wir})^{N_w - 1} - (S_w - S_{wir})^{N_w} - \frac{\epsilon - S^*}{S^*} (S^* - S_{wir})^{N_w},$$

is nonnegative for all $S_w > S^*$. To study the sign of F , rewrite it in the form

$$F(S_w, \epsilon) = (\epsilon - S^* + S_{wir})(S_w - S_{wir})^{N_w - 1} - \frac{\epsilon - S^*}{S^*} (S^* - S_{wir})^{N_w},$$

and note that F is monotone in S_w and, moreover, $F(S^*, \epsilon) > 0$ for $S^* > S_{wir}$, which is the case considered here. Thus, if $\epsilon > S^* - S_{wir}$, the function F is non decreasing and $F > 0$ for all $S_w > S^*$, so the necessary condition is fulfilled.

One can show that if $\epsilon \leq S^* - S_{wir}$, the function is non increasing and the sign depends on S_w , so that it is always possible to find a Corey coefficient N_w such that the necessary condition is not satisfied, leading to an ill-posed problem. Therefore, $\epsilon = S^* - S_{wir}$ is an optimal choice in the sense that every smaller value will result in an ill-posed problem, and every greater value will allow more polymer to enter the inaccessible pore volume. Hence, the following values of ϵ are chosen depending on the irreducible and inaccessible pore volume saturations:

$$\epsilon = \begin{cases} 0 & \text{if } S^* \leq S_{wir}, \\ S^* - S_{wir} & \text{if } S^* > S_{wir}. \end{cases} \quad (5.55)$$

The appropriate value of ϵ is then inserted into (5.53) to obtain the velocity enhancement factor. A plot of $\alpha(S_w)$ for different values of Corey's coefficient N_w is shown in

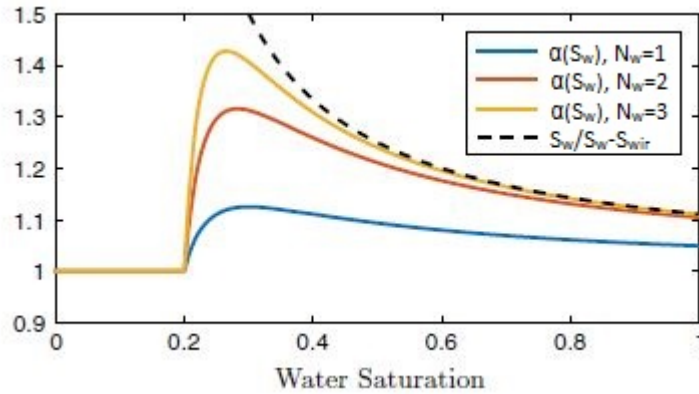


Figure 5.9: Example of a probability distribution showing the threshold radius and the three different phases. From [14].

figure 5.9. Note that the curves of the velocity enhancement factor are shown to stay below the upper limit given by the necessary condition.

Numerical simulations are performed for a one-dimensional problem to test the behaviour of the solution and compare the proposed models, paying particular attention whether the polymer concentration profile will exhibit a peak right after the shock. The examined models are the conventional model (constant velocity enhancement factor), percolation model (proposed by Bartelds), uniform polymer diffusion model and non-uniform polymer diffusion model with relaxed definition of inaccessibility. Four different scenarios are simulated, using a unit length domain (1 m), homogeneous permeability and $\phi = 0.3$. 0.25 pore volumes of water with dissolved polymer are injected at $x = 0$. Concentration of the injected polymer is 1 kg/m^3 . All the simulation results are shown in figure 5.10.

In the first case, relative permeabilities are taken to be linear in the water saturation and $S_{w,ipv} > S_{wir}$. In addition, water viscosity is set to be unaffected by the presence of polymer, which is thus considered to behave as an inert component. The water saturation profile is the same for all the four models as the viscosity is not affected by the polymer. Since the relative permeabilities are linear, the solution results in a pure shock. The conventional and percolation model show a sharp peak, which appears to grow unbounded, at the water front. The uniform and non-uniform models do not show such peak.

In the second example, the settings are the same as in the previous case, except that the relative permeabilities are now quadratic functions of the saturation. The water saturation profile is again the same for all the models, showing this time the typical Buckley-Leverett front. The conventional model shows a smooth accumulation of the polymer at the front, while both percolation and uniform models exhibit a sharper spike. The non-uniform model is observed to give a monotone concentration profile.

In the third example, the polymer is no longer considered as an inert component and $S_{w,ipv} < S_{wir}$. The only model showing accumulation of the polymer is the conventional one, while the other models give the same result as in this case $S_{w,ipv} < S_{wir}$, so they reduce to the same expression for the velocity enhancement factor.

Last, the same scenario of example three is considered, except that now $S_{w,ipv} > S_{wir}$. The non-uniform model is the only one that does not show a pile-up of the polymer at the front, while the percolation and uniform models result in a sharp

peak in polymer concentration. The profile of the conventional model is similar to example three.

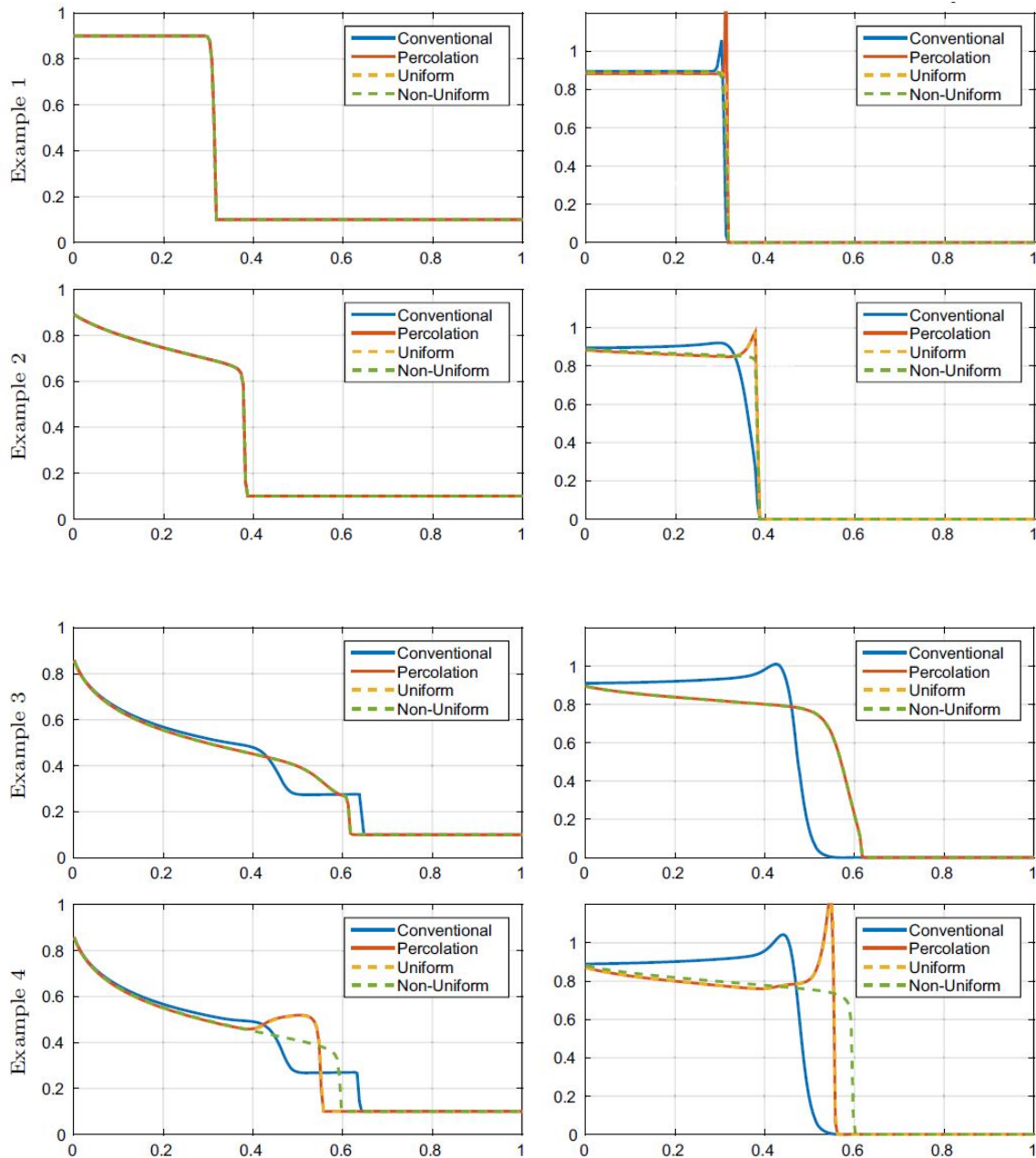


Figure 5.10: Numerical solutions for water saturation (left) and polymer concentration (right) using the four different models for $\alpha(S_w)$. From [14].

5.2.4. Conclusions

Several models for the velocity enhancement factor have been proposed. It was shown that a constant factor leads to an ill-posed model and the numerical simulations may show a peak in polymer concentration at the polymer front. This peak grows uncontrolled depending on the grid size adopted for the numerical method, so it motivates to derive more accurate models that can prevent stability issues. A model based on a percolation approach to predict IPV effects was first derived by Bartelds. Such model

is shown to be well-posed³, but it is subject to the restriction that the inaccessible water saturation is smaller than the connate water saturation. In practical situations, we are not guaranteed that this will always be the case. Therefore, Hilden et al. proposed a model that relaxes this restriction. In this model, a small fraction of polymer is allowed to enter the inaccessible pore volumes. Numerical simulations show that the latter model results in a monotone profile for the polymer concentration, which is appealing from a numerical point of view since it may avoid stability problems. On the other hand, a monotone solution may not be the actual physical solution: since polymer is allowed to travel faster than water, one might expect an accumulation at the front. Bartelds [2] reported several physical experiments where a higher polymer concentration right after the water breakthrough was observed at the effluent. Bartelds claims though that the main cause of polymer accumulation is the EPV effect, which was not taken into account by the model proposed by Hilden. Moreover, Hilden's model disregards adsorption and dispersion, focusing mainly on the IPV effects, but when considering a real reservoir these physical phenomena have to be taken into account.

In conclusion, modeling IPV effects presents mathematical and numerical challenges which will be further investigated. A constant velocity enhancement factor should be avoided, since it causes unbounded peaks in concentration which depends on the grid cells. The model proposed by Hilden et al. shows a regular and monotone profile, but it seems to exclude the presence of a polymer pile-up at the front, which may actually be a physical scenario. Caution must then be exercised when deciding which model to employ in the reservoir simulator: Hilden model will give a more conservative solution in the sense that, to preserve numerical stability, it might cut a physical polymer peak at the front. To obtain a more realistic model, EPV and adsorption have to be inserted in the model as well.

³here well-posedness is intended in the sense that the resulting system of governing equations is strictly hyperbolic.

6

Overview of Numerical Methods

Except for very simple cases, analytical solutions for water saturation and polymer concentration profiles are not available and therefore numerical methods are needed. Sintef provides a Matlab simulation toolbox (MRST, Matlab Reservoir Simulation Toolbox) in order to simulate the flow both in the case of a waterflood or polymer flood. This toolbox uses a finite volume discretization in space with first order upwind schemes for the fluxes and an implicit discretization in time in order to avoid stability issues. Equations are rewritten in conservation form and then discretized. In this chapter, the numerical scheme used by the MRST toolbox is presented first for the waterflood case. The method is then extended to the polymer flood, where the water and polymer equations are coupled and solved simultaneously using a fully implicit first order upwind method. Although this approach yields an unconditionally stable method, it introduces a strong numerical diffusion and, moreover, it is computationally expensive since equations are non-linear and must be solved using the Newton method. Thus, an alternative approach was proposed in [7]. Focusing first on the transport of an inert tracer (so that the transport equation is decoupled from the flow equations), explicit and semi-implicit methods are studied and higher-resolution methods are employed to improve the accuracy of the solution. High-resolution methods are then extended to polymer flooding, solving the equations sequentially: flow equations are solved with the old concentration value, while the polymer continuity equation is solved using the current value for the water saturation.

In industrial simulators, a constant factor for the velocity enhancement is usually used, even if it is known that the model is not well-posed and the concentration profile might result in sharp peaks at the polymer front, as showed in the previous chapter. In a recent paper, Braconnier et al. [1] showed that using an IMPES (Implicit pressure explicit saturation) scheme with first order upwind method will result in a non-monotonous concentration profile.

Information presented in the following sections are taken from [7].

6.1. Numerical Methods for Waterflooding

The one-dimensional domain $[0, L]$ is discretized into N equal sized control volumes V_j , $j = 1, \dots, N$, $|V_j| = \Delta x$, using a cell-centered discretization. Cell centers are denoted by x_j (see figure 6.1). Equations for water and oil in conservation form and with

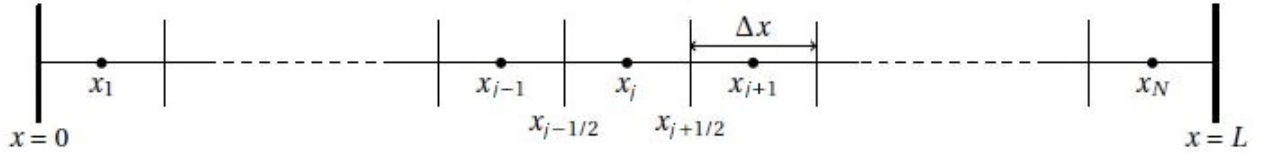


Figure 6.1: Cell-centered grid.

incompressibility assumption are recalled to be

$$\frac{\partial}{\partial t}(\phi S_\alpha) + \frac{\partial}{\partial x}(u_\alpha) = 0, \quad \alpha \in \{o, w\}. \quad (6.1)$$

Disregarding capillary pressures, integration of the spatial derivative (6.1) over a control volume gives

$$\int_V \frac{\partial}{\partial x}(u_\alpha) dx = - \int_V \frac{\partial}{\partial x} \left(\lambda_\alpha \frac{\partial p}{\partial x} \right) = - \left[\lambda_\alpha \frac{\partial p}{\partial x} \right]_{x_{j-1/2}}^{x_{j+1/2}} = -(F_{\alpha, j+1/2} - F_{\alpha, j-1/2}), \quad (6.2)$$

where $F_{\alpha, j+1/2}$ and $F_{\alpha, j-1/2}$ represent the fluxes through the right and left boundaries, respectively. The pressure derivative is discretized using a backward difference scheme

$$\left. \frac{\partial p}{\partial x} \right|_{x_{j+1/2}} \approx \frac{p_{j+1} - p_j}{\Delta x},$$

while the mobility $\lambda_\alpha(S_\alpha)$ is discretized through a first order upwind scheme. Since water is injected at $x = 0$, the flow is from left to right and the upwind approximation reads

$$\lambda_{\alpha, j+1/2} = \lambda_\alpha(S_{\alpha, j+1/2}) \approx \lambda_\alpha(S_{\alpha, j}) = \frac{kk_{r, \alpha}(S_{\alpha, j})}{\mu_\alpha}.$$

For the time derivative of (6.1), a first order backward scheme with time step Δt gives

$$\frac{\partial}{\partial t}(\phi S_\alpha) \approx \phi \frac{S_\alpha^{n+1} - S_\alpha^n}{\Delta t}.$$

Integration over a control volume V_j and mean value theorem lead to the fully implicit discretized form of equation (6.1)

$$\phi \Delta x \frac{S_{\alpha, j}^{n+1} - S_{\alpha, j}^n}{\Delta t} = \left(\lambda_{\alpha, j}^{n+1} \frac{p_{j+1}^{n+1} - p_j^{n+1}}{\Delta x} - \lambda_{\alpha, j-1}^{n+1} \frac{p_j^{n+1} - p_{j-1}^{n+1}}{\Delta x} \right). \quad (6.3)$$

Since the mobilities are non-linear functions of the saturation, Newton method is used to solve the discrete system. Rewriting (6.3) in the residual form

$$R_{\alpha, j} = \phi \Delta x \frac{S_{\alpha, j}^{n+1} - S_{\alpha, j}^n}{\Delta t} - \left(\lambda_{\alpha, j}^{n+1} \frac{p_{j+1}^{n+1} - p_j^{n+1}}{\Delta x} - \lambda_{\alpha, j-1}^{n+1} \frac{p_j^{n+1} - p_{j-1}^{n+1}}{\Delta x} \right) = 0,$$

the system of discretized equations that must be solved is

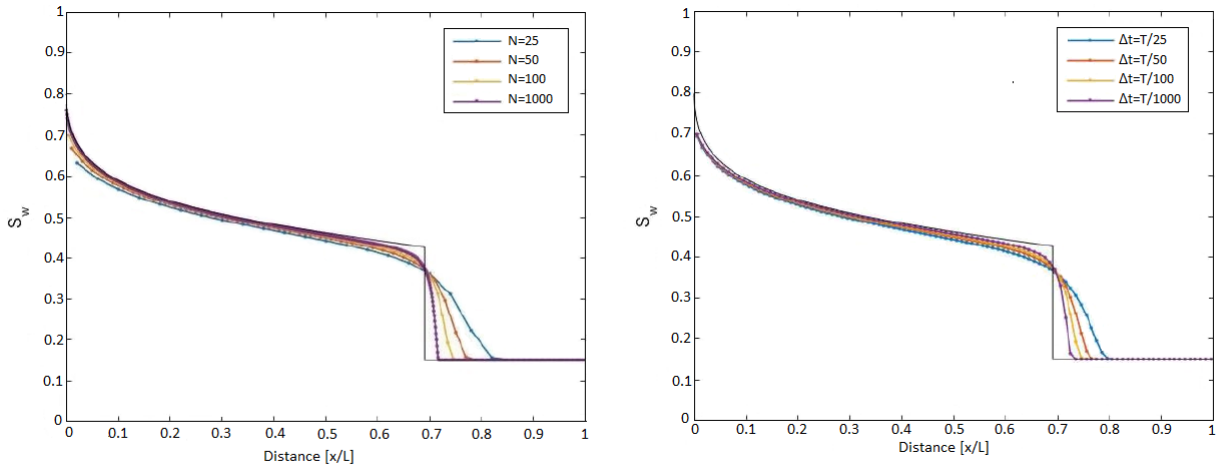
$$\mathbf{R}(\mathbf{x}^{n+1}, \mathbf{x}^n) = 0,$$

where \mathbf{x} is the vector containing the unknowns. The Newton scheme solves the following system at each iteration:

$$\frac{d\mathbf{R}}{d\mathbf{x}}\delta\mathbf{x}^{k+1} = -\mathbf{R}(\mathbf{x}^k), \quad k = 0, 1, \dots,$$

updating at each step $\mathbf{x}^{k+1} = \delta\mathbf{x}^{k+1} + \mathbf{x}^k$. The iterations continue until $\|\mathbf{R}(\mathbf{x}^k)\|_\infty < \epsilon$, where ϵ is some given tolerance. The analytical expression of the Jacobian $\frac{d\mathbf{R}}{d\mathbf{x}}$ may be extremely expensive to compute. The MRST simulator uses automatic differentiation to prevent this problem: all operations applied to the variables are also applied to their derivatives in differential form.

The implicit scheme used by the MRST simulator is unconditionally stable, but this comes at the expenses of accuracy. The water front might be severely smeared out at the discontinuity. Furthermore, Taylor series expansion cannot be carried out at the discontinuity since it requires the function to be smooth, so at the shock the order of accuracy is even less than one. For these reasons, explicit and semi-implicit schemes will be briefly discussed when discretizing the polymer continuity equation. These schemes are usually less computationally intensive than implicit schemes, but restriction on the time step are needed in order to ensure stability. To improve accuracy, higher order fluxes will also be considered. Figure 6.2 shows how the implicit solver fails to capture the discontinuity accurately and smears out the water saturation profile.



(a) Saturation profiles for $\Delta t = T/100$.

(b) Saturation profiles for $N = 100$.

Figure 6.2: Solution for the water saturation using the fully implicit solver and different values of time step and grid cells [7].

6.2. Numerical Methods for Inert Tracer

Before dealing with numerical schemes for polymer flooding, it may be useful to investigate the case of transport of an inert tracer in order to gain insights on the behaviour of explicit and semi-implicit schemes, as well as higher-resolution methods, when applied to an uncoupled transport equation. Water properties are not affected by the presence of the tracer, so that the fractional flow function depends only on

water saturation. The transport equation for the tracer concentration c is

$$\frac{\partial}{\partial t}(\phi c S_w) + \frac{\partial}{\partial x}(c u_w) = 0. \quad (6.4)$$

First, the flow is solved with the fully implicit method. Then, the obtained discrete values of u_w and S_w are used to solve the transport equation.

Similarly to the previous section, a finite volume discretization combined with a first order backward time scheme results in

$$\phi \Delta x \frac{(c S_w)_j^{n+1} - (c S_w)_j^n}{\Delta t} = -(F_{j+1/2} - F_{j-1/2}), \quad (6.5)$$

where the fluxes $F_{j\pm 1/2}$ are again approximated by a first order upwind scheme. Three approaches are compared:

- Explicit

$$F_{j+1/2} = F_{j+1/2}^n = (c_j^n u_{w,j}^n),$$

- Semi-implicit

$$F_{j+1/2} = (c_j^n u_{w,j}^{n+1}),$$

- Implicit

$$F_{j+1/2} = F_{j+1/2}^{n+1} = (c_j^{n+1} u_{w,j}^{n+1}).$$

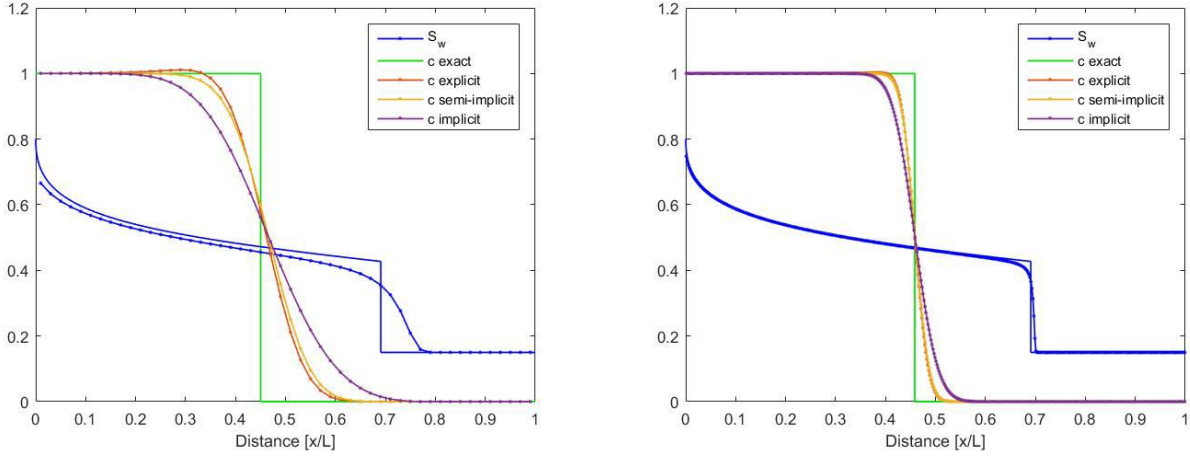
Equation (6.5) is solved for the unknown $(c S_w)_j^{n+1}$ and the concentration is found as $c_j^{n+1} = \frac{(c S_w)_j^{n+1}}{S_{w,j}^{n+1}}$. If $S_{w,j}^{n+1}$ is close to zero, this term is replaced by a value ϵ in order to avoid numerical issues which can lead to unphysical solutions.

Numerical solutions for the three cases are shown in figure 6.3. The explicit and semi-implicit methods reduce the numerical diffusion, but the front is still severely smeared out. Moreover, the explicit scheme results in a non-monotonous profile, which is non physical. It can be shown that the explicit scheme is monotonicity-preserving only if the underlying flow is also solved by an explicit scheme satisfying a CFL condition. Monotonicity for the semi-implicit scheme can be guaranteed by imposing restriction on the time step, which may though be much stricter than the CFL condition for small values of S_w . For a thorough analysis of the monotonicity, refer to [7].

To reduce the numerical diffusion, high-resolution methods are introduced. The idea of these methods is to use a higher order scheme for the fluxes, switching to a first order scheme near the discontinuity. This approach is well suited for advection problems since first order upwind smears out the solution, while higher order schemes result in oscillations close to the jump. The high resolution methods considered here are the total variation diminishing (TVD) flux-limiter methods, i.e. methods for which the total variation (of the concentration)

$$TV(c) = \sum_{j=1}^N |c_j - c_{j-1}|$$

does not grow over time, meaning that $TV(c^{n+1}) \leq TV(c^n)$. Such methods guarantee that no unphysical oscillations will arise in the solution.



(a) Solution with 50 grid cells and time steps.

(b) Solution with 500 grid cells and time steps.

Figure 6.3: Solutions for water saturation and normalized concentration using the explicit, semi-implicit and implicit methods [7].

The expression of the flux will then take the form

$$F_{j+1/2} = F_{L,j+1/2} + \Phi_{j+1/2}(F_{H,j+1/2} - F_{L,j+1/2}), \quad (6.6)$$

where F_L is the low order flux given by the above upwind scheme, F_H the higher order flux given by the second order upwind scheme

$$F_{H,j+1/2} = \frac{1}{2}u_{w,j}(c_j + c_{j+1}) - \frac{1}{2}(u_{w,j})^2 \frac{\Delta t}{\Delta x}(c_{j+1} - c_j),$$

and $\Phi = \Phi(\theta_{j+1/2})$ the flux limiter function, where

$$\theta_{j+1/2} = \frac{c_j - c_{j-1}}{c_{j+1} - c_j}$$

so that, far away from the discontinuity, $\theta_{j+1/2} \approx 1$ and $\Phi(1) = 1$, while close the discontinuity $\theta_{j+1/2} \approx 0$ and $\Phi(0) = 0$. TVD flux limiters must be used in order to have a TVD scheme. One of the most common TVD limiter is the van Leer one, defined by

$$\Phi(\theta) = \frac{\theta + |\theta|}{1 + |\theta|}. \quad (6.7)$$

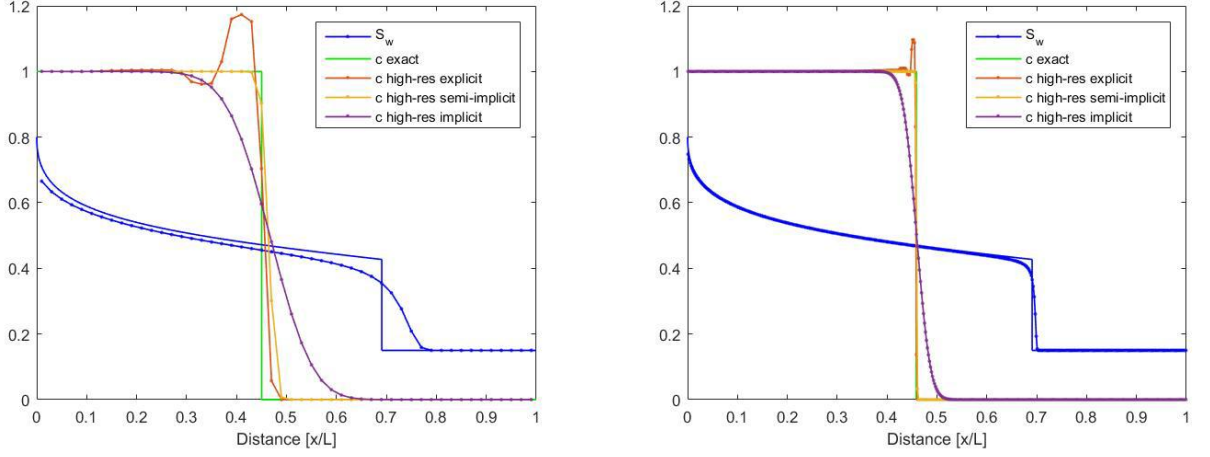
Again, the three cases with explicit, semi-implicit and implicit schemes are compared. The resulting fluxes are:

- Explicit

$$F_{j+1/2} = F_{j+1/2}^n = c_j^n u_{w,j}^n + \Phi(\theta_{j+1/2}^n) \frac{1}{2} u_{w,j}^n \left(1 - \frac{\Delta t}{\Delta x} u_{w,j}^n \right) (c_{j+1}^n - c_j^n),$$

- Semi-implicit

$$F_{j+1/2} = c_j^n u_{w,j}^{n+1} + \Phi(\theta_{j+1/2}^n) \frac{1}{2} u_{w,j}^{n+1} \left(1 - \frac{\Delta t}{\Delta x} u_{w,j}^{n+1} \right) (c_{j+1}^n - c_j^n),$$



(a) Solution with 50 grid cells and time steps.

(b) Solution with 500 grid cells and time steps.

Figure 6.4: Solutions for water saturation and normalized concentration using the explicit, semi-implicit and implicit high-resolution methods [7].

- Implicit

$$F_{j+1/2} = F_{j+1/2}^{n+1} = c_j^{n+1} u_{w,j}^{n+1} + \Phi(\theta_{j+1/2}^{n+1}) \frac{1}{2} u_{w,j}^{n+1} \left(1 - \frac{\Delta t}{\Delta x} u_{w,j}^{n+1} \right) (c_{j+1}^{n+1} - c_j^{n+1}).$$

While the explicit and semi-implicit methods are linear for c_j^{n+1} , the implicit scheme results in a non-linear iteration for c_j^{n+1} , so that Newton's method has to be used to solve the non-linear system.

Simulation results are shown in figure 6.4. The semi-implicit high-resolution scheme performs best, strongly reducing the numerical diffusion. The explicit scheme seems to have stability issues, since close to the discontinuity the concentration profile presents oscillations. As mentioned before, in order to achieve stability when using explicit fluxes, strict restriction on the time step are needed. The implicit scheme has the advantage of being unconditionally stable, but the numerical diffusion smears out the solution even with higher order fluxes. Moreover, due to the non-linearity, this scheme is the most expensive of the three. To conclude, the semi-implicit high-resolution scheme is the most efficient method in term of accuracy and computation time. The method is TVD, so it is stable provided that the CFL condition holds. Using the method of frozen coefficients and Von Neumann analysis, a local stability criterion for the transport equation in the form of CFL condition is found to be

$$C_T = \frac{\Delta t}{\Delta x} |v_{max}| = \max_{S_w} \left| \frac{\Delta t}{\phi \Delta x} \frac{u_w(S_w)}{S_w} \right| \leq 1, \quad (6.8)$$

where v_{max} is the maximum wave speed encountered and C_T is the Courant number. If the restriction on the time step becomes too strict, it is safer to switch to the implicit scheme.

A monotonicity analysis shows that the explicit scheme preserves a monotone profile only if the underlying flow is also solved through explicit fluxes and a CFL-type condition holds. The semi-implicit scheme is conditionally monotonicity-preserving, but the time step restriction may be significantly stricter than the CFL condition,

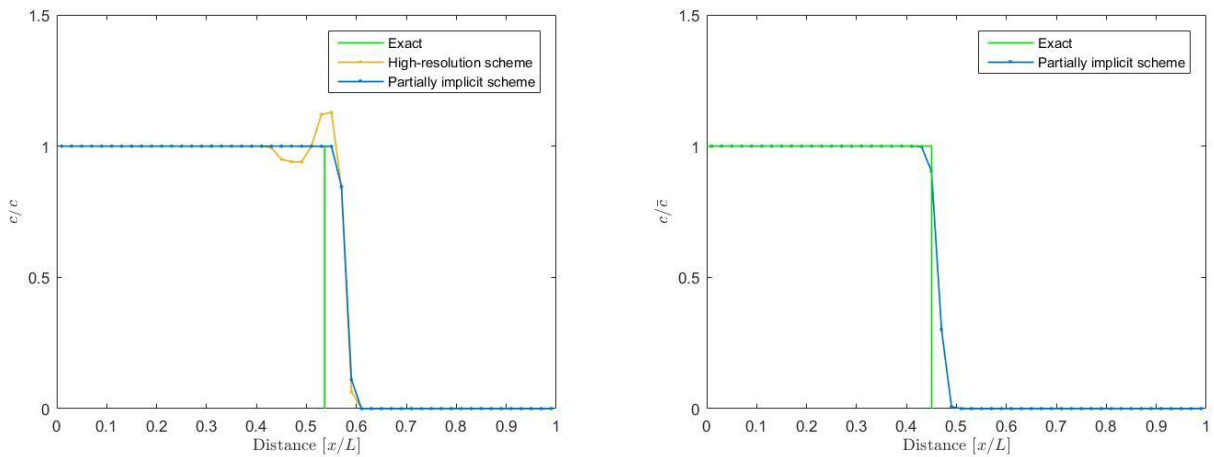
especially for small values of S_w . On the other hand, the implicit scheme results in an unconditionally monotonous profile, but it is the most expensive of the three methods and, moreover, there is no relevant gain in accuracy by switching from a first order to a higher order implicit method. Therefore, a good strategy would be to use the semi-implicit high resolution method and switch to a monotonous first order implicit scheme close to the discontinuity. The resulting partially implicit scheme can be written as

$$(cS_w)_j^{n+1} = (cS_w)_j^n - \frac{\Delta t}{\phi \Delta x} (1 - \beta_j) (F_{j+1/2}^n - F_{j-1/2}^n) - \frac{\Delta t}{\phi \Delta x} \beta_j (F_{j+1/2}^{n+1} - F_{j-1/2}^{n+1}), \quad (6.9)$$

where $F_{j\pm 1/2}^n$ are the semi-implicit high resolution fluxes and $F_{j\pm 1/2}^{n+1}$ are the implicit first order fluxes. The coefficient β_j denotes the degree of implicitness in cell j . If $\beta_j = 1$ for all j , then (6.9) reduces to the first order implicit scheme, while if $\beta_j = 0$ for all j , (6.9) reduces to the semi-implicit high resolution scheme. The concentration profile is monotonous if $c_{j+1}^{n+1} \leq c_j^{n+1}$ for all j . One can show that this condition is equivalent to require that, for the semi-implicit first order scheme,

$$\frac{\Delta t}{\phi \Delta x} u_{j+1}^{n+1} \leq S_{w,j+1} \quad (6.10)$$

holds. Therefore, we choose $\beta_j = 0$ when (6.10) holds and $\beta_j = 1$ elsewhere. Stability condition for the partially implicit method is the one required by the semi-implicit scheme. Simulation results are shown in figure 6.5. The partially implicit scheme maintains a monotonous profile. However, the accuracy gets worse as the value of S_{wc} is smaller. This is because for low values of S_{wc} , the water and tracer fronts are close to each other and the water saturation profile is solved implicitly, meaning that numerical diffusion will smear its profile. As a consequence, the low accuracy of the water profile at the front will result in a less accurate profile for the concentration as well.



(a) Solution with $S_{wc} = 0.015$.

(b) Solution with $S_{wc} = 0.15$.

Figure 6.5: Solutions for normalized concentration using the partial implicit high-resolution method [7].

6.3. Numerical Methods for Polymer Flooding

Adding a polymer to the injected water will influence chemical and physical properties of the fluid. In this case, continuity equation for water saturation and polymer concentration are coupled. The MRST simulator solves the equations simultaneously with a fully implicit first order upwind method. This approach result in the following scheme

$$\begin{cases} S_{o,j}^{n+1} &= S_{o,j}^n - \frac{\Delta t}{\phi \Delta x} \left(u_o(S_{o,j}^{n+1}, c_j^{n+1}) - u_o(S_{o,j-1}^{n+1}, c_{j-1}^{n+1}) \right), \\ S_{w,j}^{n+1} &= S_{w,j}^n - \frac{\Delta t}{\phi \Delta x} \left(u_w(S_{w,j}^{n+1}, c_j^{n+1}) - u_w(S_{w,j-1}^{n+1}, c_{j-1}^{n+1}) \right), \\ (cS_w)_j^{n+1} &= (cS_w)_j^n - \frac{\Delta t}{\phi \Delta x} \left(c_j^{n+1} u_w(S_{w,j}^{n+1}, c_j^{n+1}) - c_{j-1}^{n+1} u_w(S_{w,j-1}^{n+1}, c_{j-1}^{n+1}) \right). \end{cases}$$

Although it has the advantage to be a more stable scheme, accuracy is low due to the first order upwind fluxes, and the non linearities in both S_w and c makes it computationally expensive. For this reason, an alternative sequential approach has been proposed: the flow equations are solved implicitly using the value of concentration at time level n and subsequently the polymer continuity equation is solved using the updated value of S_w . The scheme reads:

1. Compute S_w^{n+1} using c^n and the fully implicit solver:

$$\begin{cases} S_{o,j}^{n+1} = S_{o,j}^n - \frac{\Delta t}{\phi \Delta x} \left(u_o(S_{o,j}^{n+1}, c_j^n) - u_o(S_{o,j-1}^{n+1}, c_{j-1}^n) \right) \\ S_{w,j}^{n+1} = S_{w,j}^n - \frac{\Delta t}{\phi \Delta x} \left(u_w(S_{w,j}^{n+1}, c_j^n) - u_w(S_{w,j-1}^{n+1}, c_{j-1}^n) \right). \end{cases}$$

2. Compute c^{n+1} using S_w^{n+1}

$$(cS_w)_j^{n+1} = (cS_w)_j^n - \frac{\Delta t}{\phi \Delta x} \left(F_{j+1/2}(S_w^{n+1}, c^n, c^{n+1}) - F_{j-1/2}(S_w^{n+1}, c^n, c^{n+1}) \right).$$

In order to complete the scheme, an expression for the fluxes $F_{j\pm 1/2}$ must be selected. Given the discussion of the previous section, two high-resolution methods are compared:

- Semi-implicit high-resolution

$$F_{j+1/2} = c_j^n u_{w,j}^{n+1} + \Phi(\theta_{j+1/2}^n) \frac{1}{2} u_{w,j}^{n+1} \left(1 - \frac{\Delta t}{\Delta x} u_{w,j}^{n+1} \right) (c_{j+1}^n - c_j^n),$$

- Implicit high-resolution

$$F_{j+1/2} = F_{j+1/2}^{n+1} = c_j^{n+1} u_{w,j}^{n+1} + \Phi(\theta_{j+1/2}^{n+1}) \frac{1}{2} u_{w,j}^{n+1} \left(1 - \frac{\Delta t}{\Delta x} u_{w,j}^{n+1} \right) (c_{j+1}^{n+1} - c_j^{n+1}).$$

Results are shown in figures 6.6 and 6.7. Again, the semi-implicit scheme seems to perform best in term of accuracy, while the implicit scheme smears the water saturation profile at the polymer front and the concentration profile.

A stability criterion for the semi-implicit scheme similar to (6.10) can be found via Von Neumann analysis giving the necessary condition

$$C_p = \max_{S_w, c} \left| \frac{\Delta t}{\phi \Delta x} \frac{u_w(S_w, c)}{S_w} \right| = \max_{S_w, c} \left| \frac{\Delta t}{\Delta x} \frac{u_T}{\phi} \frac{f_w(S_w, c)}{S_w} \right| \leq 1. \quad (6.11)$$

Since the fractional flow curve shifts to the right when polymer is added to water, the above maximum is attained at $c = 0$, so that condition (6.11) is equivalent to (6.8).

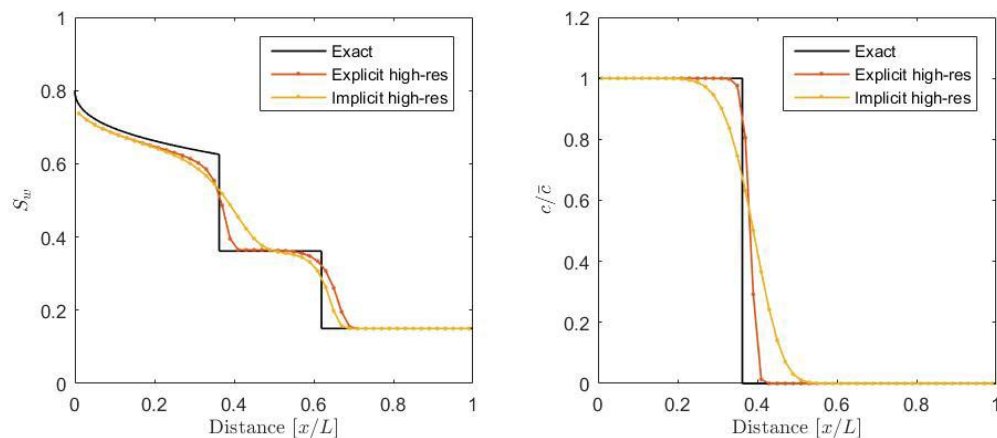


Figure 6.6: Solutions water saturation for normalized concentration using high-resolution methods and 50 cells and time steps [7].

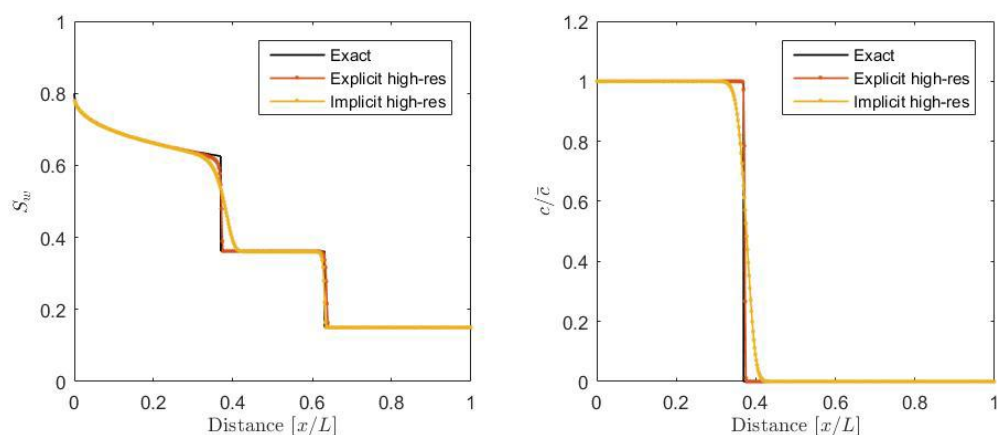


Figure 6.7: Solutions for water saturation normalized concentration using high-resolution methods and 500 cells and time steps [7].

6.4. Remarks on Velocity Enhancement Factor

The numerical methods presented in the current chapter have been applied to polymer flooding disregarding the velocity enhancement effect. The model factor $\alpha(S_w)$ can be incorporated into the schemes, but, as discussed in chapter 5, it is not clear which model is well-suited to describe the underlying physical phenomenon. Moreover, stability issues arise when inserting the velocity enhancement factor into the model. It has been shown that a constant factor results in an ill-posed model which causes an unlimited pile-up of the polymer at the front. The alternative models proposed address the ill-posedness and succeed to obtain a monotonous profile of the polymer concentration, but there is no guarantee that these are indeed the correct physical solutions.

Currently, most of the industrial simulators, and in particular the MRST simulator, are still using a constant factor to model the inaccessible pore volume effect. A more detailed analysis of the consequences of a constant velocity enhancement factor on a numerical scheme have been investigated in [1]. Solving the system of equations through finite volumes with first order upwind fluxes and an explicit scheme in time, they performed a stability analysis for the water saturation and polymer concentration profiles. They derived CFL-type conditions, i.e. restrictions on the time step,

in order to guarantee that the water saturation will remain in its definition interval $[S_{wc}, 1 - S_{or}]$ and that the polymer concentration c will be positive. Furthermore, it is shown that the numerical scheme for the concentration is potentially non-monotone due to a term that arises when a constant velocity enhancement factor is introduced. The simulation results presented in the paper show the typical peak at the polymer front when inaccessible pore volume is considered.

The future work will be devoted to improve the current models used for polymer flooding when the inaccessible pore volume effect is included, considering the more recent analytical models proposed in chapter 5 and deriving a more robust numerical scheme in order to obtain more realistic simulations.

Bibliography

- [1] Braconnier B., Preux C., Flauraud É, Tran Q.H., and Berton C. An analysis of physical models and numerical schemes for polymer flooding simulations. *Computational Geoscience*, 21:1267–1279, 2017.
- [2] Gepke Alies Bartelds. *The influence of inaccessible and excluded pore volume in polymer flooding*. PhD thesis, Delft University of Technology, 1998.
- [3] Bartelds G.A., Bruining J., and Molenaar J. The modeling of velocity enhancement in polymer flooding. *Transport in porous media*, 26(1):75–88, 1997.
- [4] Holden H. and Risebro N.H. *Front tracking for hyperbolic conservation laws*. 2nd edn. Springer, Heidelberg, 2015.
- [5] Aziz K. and Settari A. *Petroleum Reservoir Simulations*. Elsevier Applied Science, London, 1979.
- [6] Sorbie K.S. *Polymer-Improved Oil Recovery*. Blackie, Glasgow, 1991.
- [7] Wiegman L. Numerical aspects of transport modelling in enhanced oil recovery. Master’s thesis, Delft University of Technology, 2017.
- [8] Lake L.W., Johns R.T., Rossen W.R., and Pope G. *Fundamentals of Enhanced Oil Recovery*. Society of Petroleum Engineers, 2014.
- [9] Todd M.R. and Longstaff W.J. The development, testing, and application of a numerical simulator for predicting miscible flood performance. *Journal of Petroleum Engineering*, 24(7):874–882, 1972.
- [10] Gary A. Pope. The application of fractional flow theory to enhanced oil recovery. *Society of Petroleum Engineers journal*, 20:191–205, 1980.
- [11] Dawson R., Lantz R.B., and Aime M. Inaccessible pore volume in polymer flooding. *Society of Petroleum Engineers journal*, 12(5):448–452, 1972.
- [12] Salsa S. *Partial Differential Equations in Action. From Modelling to Theory*. Springer, 2008.
- [13] Buckley S.E. and Leverett M.C. Mechanism of fluid displacement in sands. *Trans AIME*, 146(1):107–116, 1942.
- [14] Hilden S.T., Nilsen H.M., and Raynaud X. Study of the well-posedness of models for the inaccessible pore volume in polymer flooding. *Transport in porous media*, 114(1):65–86, 2016.
- [15] Chen Z. *Reservoir Simulation-Mathematical Techniques in Oil Recovery*. SIAM, Philadelphia, 2007.